Available online at www.sciencedirect.com
ScienceDirect
International Journal of Solids and Structures 44 (2007) 4418–4441
INTERNATIONAL JOURNAL OF SOLIDS and STRUCTURES
www.elsevier.com/locate/ijsolstr

A symmetric over-nonlocal microplane model M4 for fracture in concrete

Giovanni Di Luzio *

Department of Structural Engineering, Politecnico di Milano, Piazza Leonardo Da Vinci 32, 20133 Milan, Italy

Received 28 June 2006; received in revised form 16 November 2006
Available online 22 November 2006

Abstract

This paper analyzes the effectiveness of a nonlocal integral-type formulation of a constitutive law such as microplane model M4 in which the yield limits soften as a function of the total strain for prediction of fracture propagation. For a correct regularization of the mathematical problems caused by the softening behavior, an ''over-nonlocal'' generalization of the type proposed by Vermeer and Brinkgreve [Vermeer, P.A., Brinkgreve, R.B.J., 1994. A new effective non-local strain measure for softening plasticity. In: Chambon, R., Desrues, J., Vardoulakis, I. (Eds.), Localization and Bifurcation Theory for Soil and Rocks, Balkema, Rotterdam, pp. 89–100.] is adopted. Moreover, the symmetric weight function, proposed by Borino et al. [Borino, G. Failla, B., Parrinello, F., 2003. A symmetric nonlocal damage theory. International Journal of Solids and Structure 40, 3621–3645.] for damage mechanics, is introduced for the calculation of the nonlocal averaging of the total strain upon which the yield limits depend. The capability of the proposed model for reproducing the stress and strain fields in the vicinity of a notch is also investigated. Finally, the symmetric over-nonlocal generalization of microplane model M4 has been applied for the simulation of a mixed-mode fracture test such as the four-point-shear test and the test of axial tension at constant shear force [Nooru-Mohamend, M.B., 1992. Mixed-mode fracture of concrete: an experimental approach. Doctoral Thesis Delft University of Thechnology, Delft, The Netherlands.]

Keywords: Microplane model; Concrete; Nonlocal continuum; Fracture; Damage

1. Introduction

In recent years, there has been a great push to model the behavior of cohesive quasi-brittle materials such as concrete, exploring approaches including plasticity, continuum damage mechanics, plastic-fracturing theory, endocronic theory and a variety of combinations thereof. Nonetheless, the existing models are not able to realistically simulate the behavior of concrete under a complete spectrum of loading conditions. A class of promising and capable models are the microplane models evolved from the slip theory of plasticity, which was developed by Batdorf and Budianski (1949) on the basis of the original idea of Taylor (1938). Even if the

* Tel.: +39 0223994278; fax: +39 0223994220.
E-mail address: diluzio@stru.polimi.it

0020-7683/$ - see front matter
doi:10.1016/j.ijsolstr.2006.11.030

microplane model requires extensive computations (which are no longer an obstacle), it gains in the conceptual simplicity of a three-dimensional formulation and in a versatile data-fitting capability (Bažant and Prat, 1988; Bažant and Ožbolt, 1990; Bažant et al., 1996; Bažant et al., 2000; Caner and Bažant, 2000; Ožbolt et al., 2001). The most recent iteration of this series, microplane model M4, has shown, however, a deficient tensile behavior consisting of unrealistic lateral strains at very large uniaxial tensile strains, which, moreover, do not reduce exactly to zero. A solution of this problem, the basic idea of which was briefly outlined at a recent conference (Bažant et al., 2004), is presented in the present paper.

The finite element solutions for strain softening materials are afflicted by serious numerical problems caused by the fact that the boundary value problem becomes ill-posed. This means that the numerical calculations cease to be objective, exhibiting both pathological spurious mesh sensitivity and excessive damage localization when the mesh is refined. To recover a well-posed problem and to prevent the localization of damage into a zone of zero volume, many solutions have been proposed based on the introduction of the characteristic length of the material (Bažant, 1976; Bažant and Oh, 1983; Bažant et al., 1984; Larsy and Belytschko, 1988). One of the most successful techniques, which is physically justified by the micro-crack interactions and from the fact that the crack dimensions are not negligible (Bažant, 1994; Bažant and Jirásek, 1994), is based on the concept of nonlocal continuum, in which the stress at a given point depends not only on the strain at that point but also on the nearby strain field. The nonlocal concept was introduced in the 1960's (Eringen, 1966; Kröner, 1968) for elastic deformations and later extended to hardening plasticity. Bažant (1984a) and Bažant and Chang (1984) introduced the nonlocal concept as a localization limiter for a strain-softening material. This formulation was later improved in the form of the nonlocal damage theory (Pijaudier-Cabot and Bažant, 1987) and was then applied to real problems (Bažant and Lin, 1988; Bažant and Lin, 1989; Saouridis and Mazars, 1992). To refine the nonlocal formulation, Vermeer and Brinkgreve (1994) proposed a novel ''over-nonlocal'' formulation, in which the nonlocal variable is increased by a factor m larger than 1, while the corresponding local variable is reduced by the factor $(1 - m)$. The over-nonlocal formulation has been so called (Bažant and Di Luzio, 2004) because it uses a linear combination of local and nonlocal variables in which a negative weight imposed on the local variable is compensated for by assigning to the nonlocal variable a weight greater than 1. This is equivalent to a nonlocal variable with a smooth positive weight function of total weight greater than 1 normalized by superimposing a negative delta-function spike at the center.

Bažant and Di Luzio (2004) proposed a nonlocal generalization of microplane model M4 for concrete in which the yield limits, called stress–strain boundaries, are softening functions of the total strain. In the proposed nonlocal formulation, the softening yield limits are functions of the spatially averaged nonlocal strains, while the elastic strains are local. They demonstrated analytically as well as numerically that the tensile stress across the strain localization band at very large strain does soften to zero and that the cracking band retains a finite width even at very large tensile strain across the band only if one adopts an ''over-nonlocal'' generalization of the type proposed by Vermeer and Brinkgreve (1994). A complete overview on the effectiveness of various regularization techniques for softening materials, i.e., materials for which the yield limits soften as a function of the total strain, plasticity models and damage models, has been presented by Di Luzio and Bažant (2005). They verified analytically through a spectral wave propagation analysis that the nonlocal integral-type model with degrading yield limit depending on the total strain and the nonlocal integral-type plasticity model with additive format work correctly if and only if one adopts an unconventional over-nonlocal formulation. By contrast, the standard ($m = 1$) nonlocal integral-type generalization of softening plasticity with a multiplicative format provides realistic localization behavior, just like the nonlocal integral-type damage model, and thus does not necessitate an over-nonlocal formulation.

Borino et al. (2003) proposed a symmetric nonlocal damage theory in which a symmetric nonlocal integral operator was introduced. This symmetric nonlocal operator has been used for developing a symmetric over-nonlocal formulation of microplane model M4 (Di Luzio, 2004). The symmetric formulation is able to preserve the uniform fields and to reproduce a physically correct nonlocal quantity at every point of the domain, including the zones near the body boundary. This important feature is shown for a three-point-bending test in which the capability of the proposed model for reproducing a physically sound stress and strain field in the vicinity of a notch is investigated.

In the last part of the paper, the proposed symmetric over-nonlocal formulation of microplane model M4 has been applied to the simulation of the fracture propagation along a straight and a curved trajectory such as

in a classical four-point-bending test and in double-edge-notched specimen tested by Nooru-Mohamend (1992).

2. The nonlocal formulations

The primary characteristic of a nonlocal model is the replacement of a certain local variable $f(\mathbf{x})$, characterizing the softening damage of material, by its nonlocal counterpart $\overline{f}(\mathbf{x})$. The nonlocal variable is defined as

$$\overline{f}(\mathbf{x}) = \int_V \alpha^*(\mathbf{x},\boldsymbol{\xi}) f(\boldsymbol{\xi})\,\mathrm{d}V(\boldsymbol{\xi}), \tag{1}$$

where V is the volume of the structure, $\mathbf{x}$, $\boldsymbol{\xi}$ are the coordinates vectors, and $\alpha^*(\mathbf{x},\boldsymbol{\xi})$ is a weight function. The weight function in Eq. (1) has the following characteristics: (1) it is a positive function, $\alpha^*(\mathbf{x},\boldsymbol{\xi}) \geqslant 0$; (2) it has its maximum value for $\mathbf{x} = \boldsymbol{\xi}$ (i.e. $r = |\mathbf{x} - \boldsymbol{\xi}| = 0$); (3) it is a monotonic decreasing function (to zero) of the distance r (the nonlocal average in a field point have a certain finite influence volume). The weight function $\alpha(\mathbf{x},\boldsymbol{\xi})$ is often taken as a bell-shaped function; its analytical expression is

$$\alpha(\mathbf{x},\boldsymbol{\xi}) = \begin{cases} \left(1 - \frac{|\boldsymbol{\xi}-\mathbf{x}|^2}{R^2}\right)^2 & \text{if } 0 \leqslant |\boldsymbol{\xi} - \mathbf{x}| \leqslant R, \\ 0 & \text{if } R \leqslant |\boldsymbol{\xi} - \mathbf{x}|, \end{cases} \tag{2}$$

where R, called the interaction radius, is proportional to the material characteristic length ℓ, $R = \rho_0 \ell$. Note that $|\mathbf{x} - \boldsymbol{\xi}| = \sqrt{(x_i - \xi_i)^2}$ and $\alpha(\mathbf{x},\mathbf{x}) = 1$. The coefficient ρ_0 is determined so that the normalizing condition is satisfied, i.e. a uniform local strain field is transformed into a uniform nonlocal strain field. Another weight function, used to facilitate the analytical solutions, is the Gauss attenuation function, which has the form $\alpha(\mathbf{x},\boldsymbol{\xi}) = \exp(-\pi|\boldsymbol{\xi} - \mathbf{x}|^2/\ell^2)$ and unbounded support (its interaction radius is $R = \infty$). For this reason in the following numerical simulations the bell-shaped function of Eq (2) has been used.

One of the requirements which we expect from the nonlocal average is that a uniform field is not influenced by the nonlocal formulation (Eq. (1)): if the local field is uniform, the nonlocal field also must be uniform. In order to satisfy this condition, Pijaudier-Cabot and Bažant (1987) proposed the following normalized nonlocal formulation:

$$\alpha^*(\mathbf{x},\boldsymbol{\xi}) = \frac{\alpha(\boldsymbol{\xi},\mathbf{x})}{V_r(\mathbf{x})} \qquad V_r(\mathbf{x}) = \int_V \alpha(\boldsymbol{\xi},\mathbf{x})\,\mathrm{d}V(\boldsymbol{\xi}) \tag{3}$$

in which $\alpha(\mathbf{x},\boldsymbol{\xi})$ is the basic nonlocal weight function, for example the bell-shaped function or the Gauss attenuation function; $V_r(\mathbf{x})$ is called the representative volume and is a constant if the unrestricted averaging domain does not tend to protrude outside the boundaries. The nonlocal formulation in Eq. (3) ensures the normalization condition

$$\int_V \alpha^*(\mathbf{x},\boldsymbol{\xi})\mathrm{d}V(\boldsymbol{\xi}) = 1 \qquad \forall \mathbf{x}. \tag{4}$$

It is worth noting that, ensuring the uniformity of constant field in the vicinity of the boundary, the nonlocal formulation in Eq. (3) is not symmetric, i.e. $\alpha^*(\mathbf{x},\boldsymbol{\xi}) \neq \alpha^*(\boldsymbol{\xi},\mathbf{x})$ in general. This lack of symmetry makes the tangent operators nonsymmetric in the original formulation of Pijaudier-Cabot and Bažant (1987). As it will be shown in the following section, the lack of symmetry in the weight attenuation function leads to an unrealistic description of the stress and strain fields where they are not uniform, for example around a notch tip of a specimen. Recently, Borino et al. (2003) proposed a new formulation of the nonlocal integral weight function given by

$$\alpha^{**}(\mathbf{x},\boldsymbol{\xi}) = \left(1 - \frac{V_r(\mathbf{x})}{V_\infty}\right)\delta(\mathbf{x},\boldsymbol{\xi}) + \frac{\alpha(\boldsymbol{\xi},\mathbf{x})}{V_\infty}, \tag{5}$$

where $\delta(\mathbf{x},\boldsymbol{\xi})$ is the Dirac delta function, $\alpha(\boldsymbol{\xi},\mathbf{x})$ is an attenuation function (Eq. (2)), $V_r(\mathbf{x})$ is the representative volume and V_∞ is the value of the representative volume far from the boundaries where it has a constant value. The first term in Eq. (5) is a local term which is activated only for points near the boundaries, while for

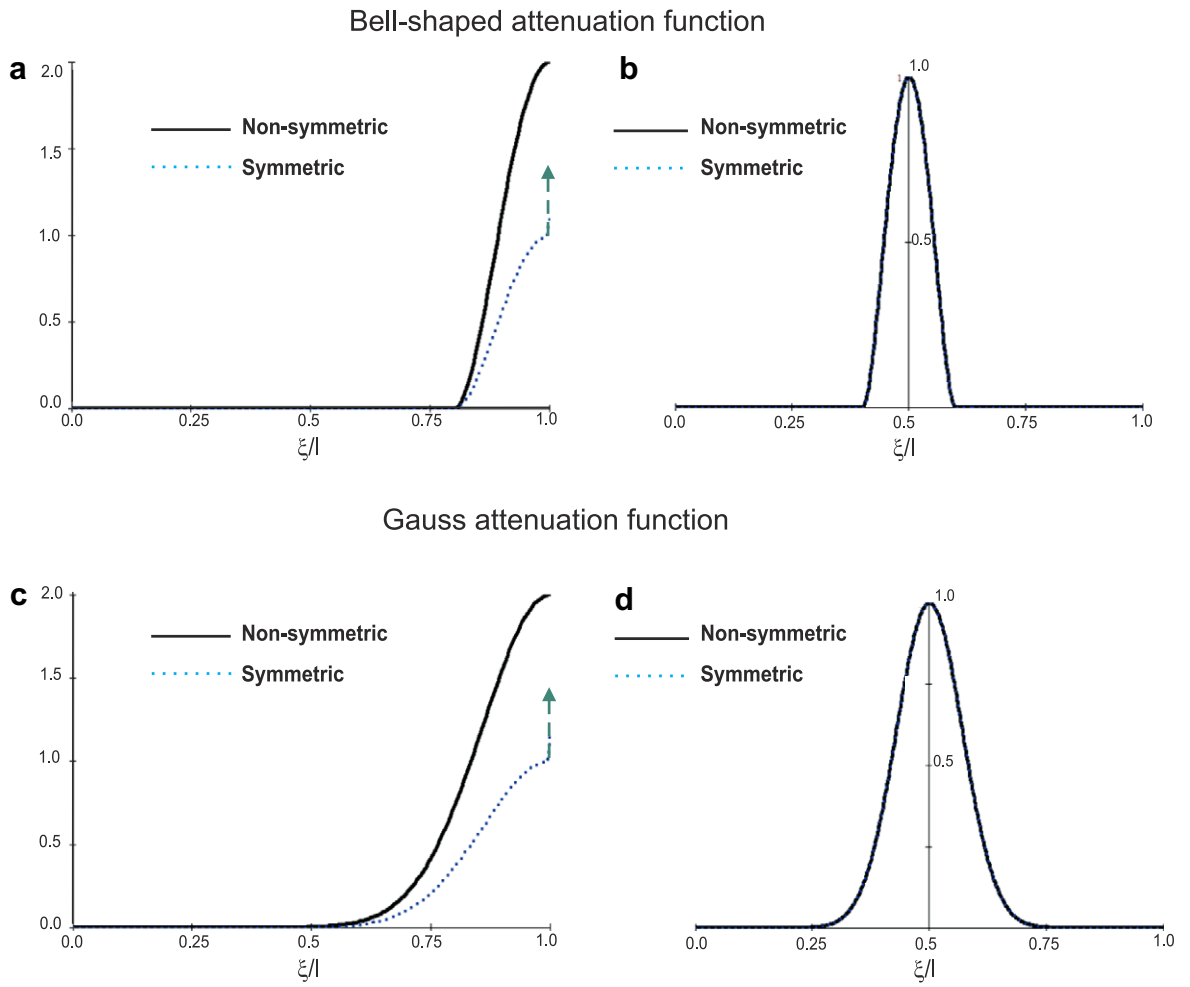

Fig. 1. One-dimensional domain ($0 \leqslant \xi/l \leqslant 1$) comparison of weight functions for symmetric and nonsymmetric nonlocal formulations: (a) weight functions for a point in right boundary using the bell shaped attenuation function with interaction radius $R = 0.2\,\mathrm{l}$; (b) weight functions for a point far from the boundary using the bell shaped attenuation function ($R = 0.2\,\mathrm{l}$); (c) weight functions for a point in right boundary using the Gauss attenuation function with internal length $\ell = 0.2\,\mathrm{l}$; (d) weight functions for a point far from the boundary using the Gauss attenuation function ($\ell = 0.2\,\mathrm{l}$).

points far from the boundaries it tends to vanish ($V_r(\mathbf{x}) \to V_\infty$). As we can see from Eq. (5), this formulation is symmetric everywhere in the domain. In particular, for an unbounded solid or for points of bounded solid sufficiently far from the boundaries, this formulation coincides with the classical nonlocal formulation, (Eq. (3)). In Fig. 1 the two different weight functions, Eqs. (3) and (5), are plotted together in a one-dimensional domain of length l for a point far from the boundary (Fig. 1b and d) and for a point located at the right boundary (Fig. 1a and c). It is clear how the two formulations, symmetric and non-symmetric, coincide for a point far from the boundaries, while they are rather different in the vicinity of the boundaries (Fig. 1a and c).

Originally Vermeer and Brinkgreve (1994) and later Planas et al. (1996) and Strömberg and Ristinmaa (1996) (see also Bažant and Planas, 1998) introduced a refinement of the standard nonlocal formulation in the form of a over-nonlocal formulation in which a combination of the local and the nonlocal variable is used

$$\hat{f}(\mathbf{x}) = m\overline{f}(\mathbf{x}) + (1-m)f(\mathbf{x}), \tag{6}$$

where $\hat{f}(\mathbf{x})$ is the over-nonlocal average of the variable $f(\mathbf{x})$, $\overline{f}(\mathbf{x})$ is the nonlocal variable obtained from Eq. (1), and m is an empirical coefficient (over-nonlocal parameter). The previous works on this formulation, con-

cerning simple softening plastic models, confirmed the avoidance of spurious localization if $m > 1$. Planas et al. (1996) then rigorously proved, for a uniaxial stress field, that the localization zone is finite if and only if $m > 1$. Later Bažant and Di Luzio (2004) showed the necessity of m greater than 1 for the nonlocal generalization of the microplane model M4. It was also proven (Bažant and Planas, 1998) that, for the uniaxial localization in a bar subjected to tension, the formulation with $m > 1$ is equivalent, in terms of strain rate, to the nonlocal damage model of Pijaudier-Cabot and Bažant (1987). Furthermore, a complete overview of the effectiveness of the over-nonlocal formulation for various softening behavior was presented by Di Luzio and Bažant (2005).

The over-nonlocal formulation can also be obtained rewriting the weight function in Eq. (1) as a function of the over-nonlocal parameter m, yielding the following equation for the non-symmetric over-nonlocal formulation

$$\alpha_m^*(\mathbf{x},\boldsymbol{\xi}) = (1-m)\delta(\boldsymbol{\xi},\mathbf{x}) + m\frac{\alpha(\boldsymbol{\xi},\mathbf{x})}{V_r(\mathbf{x})}, \tag{7}$$

where δ denotes the Dirac delta function and m is the over-nonlocal parameter (for $m = 1$ the standard nonlocal formulation is recovered). For the symmetric over-nonlocal formulation one obtains

$$\alpha_m^{**}(\mathbf{x},\boldsymbol{\xi}) = (1-m)\delta(\boldsymbol{\xi},\mathbf{x}) + m\left[\left(1-\frac{V_r(\mathbf{x})}{V_\infty}\right)\delta(\mathbf{x},\xi) + \frac{\alpha(\boldsymbol{\xi},\mathbf{x})}{V_\infty}\right]. \tag{8}$$

3. Improvements in the microplane model M4

The microplane constitutive model has the appeal of capturing the complex inelastic behavior of concrete by using simple constitutive relations between stresses and strains acting on a plane in the material called the microplane. To ensure a unique solution for a softening material, the static constraint of the *slip theory of plasticity* (Taylor, 1938), from which the microplane model is derived, has been replaced by a kinematic constraint in which the microplane strain components are calculated as the projection of the macroscopic strain tensor (Bažant, 1984b). The microplane model based on the kinematic constraint is valuable for its conceptual simplicity and three-dimensional formulation, and has shown good agreement between its predictions and experimental data (Bažant and Prat, 1988; Bažant and Ožbolt, 1990; Bažant et al., 1996; Bažant et al., 2000; Caner and Bažant, 2000; Ožbolt et al., 2001).

In the microplane model M4 based on the kinematic constraint the static equivalence (or equilibrium) of stresses between the macro and micro levels is ensured through the principle of virtual work (Bažant, 1984b). The numerical integration required is carried out according to an optimal Gaussian integration formula for a spherical surface (Stroud, 1971; Bažant and Oh, 1986). An efficient formula, which employs 21 microplanes (Bažant and Oh, 1986) and yields acceptable accuracy, has been used in this work. Other formulas with 28 (the Stroud's formula), 37 and 61 microplanes can be used to achieve better accuracy. The most general explicit constitutive relation on the microplane level gives the microplane stress components (σ_N, σ_L and σ_M) as functions of the histories of the microplane strain components (ϵ_N, ϵ_L and ϵ_M), possibly supplemented by a yield condition. However, in general, it is sufficient to assume that each of σ_N, σ_L and σ_M depends only on its corresponding strain ϵ_N, ϵ_L and ϵ_M because cross dependence on the macro level, such as shear dilatancy, is automatically captured by interaction among microplanes of various orientations (Bažant and Gambarova, 1984). An exception is the frictional yield condition relating the normal and the shear components on the microplane with no strain dependence. In the microplane model M4 (Bažant et al., 2000), the constitutive relation in each microplane is defined by (1) incremental elastic relation and (2) stress–strain boundaries (softening yield limits) that cannot be exceeded. This last condition on the stress–strain boundaries (F_N, F_V^-, F_V^+, F_D^-, F_D^+, F_T), which may be regarded as strain dependent yield limits, consists of the following conditions:

$$\sigma_N \leqslant F_N(\epsilon_N), \quad \sigma_V \geqslant F_V^-(\epsilon_V), \quad F_D^-(\epsilon_D) \leqslant \sigma_D \leqslant F_D^+(\epsilon_D), \quad \sigma_T = \sqrt{\sigma_M^2 + \sigma_L^2} \leqslant F_T(\sigma_N, \epsilon_I, \sigma_V). \tag{9}$$

Except for the last condition, which models friction, interactions among various components need not be considered, since the cross effects are adequately captured by interactions among various microplanes by means of

the kinematic constraint. The unloading conditions are formulated separately for each microplane component. The constitutive model, formulated and tested in Bažant et al. (2000) and in Caner and Bažant (2000), is completely defined on the microplane level. The original formulation of the stress–strain boundaries (Bažant et al., 2000) has been slightly changed as presented in the Appendix I.

In microplane model M2 (Bažant and Prat, 1988) the decomposition of the normal microplane components into volumetric and deviatoric part ($\sigma_N = \sigma_V + \sigma_D$ and $\epsilon_N = \epsilon_V + \epsilon_D$) was introduced to control the value of the Poisson's ratio and to model compressive failure. However, this model showed a pathological behavior for tensile failure due to the split of the normal microplane component and not to the kinematic constraint itself (Jirásek, 1993). There are two ways to eliminate this unwanted phenomenon: (1) to impose the static constraint on each microplane; (2) to introduce some modification in the formulation of the kinematic constraint approach. In this regard, the microplane model M3 (Bažant et al., 1996) introduced the softening strain-dependent limits (called stress–strain boundaries) in which the spilt of the normal component is not fixed a priori, but imposed by the normal boundary independently for each microplane depending on the current strain. The model basically eliminates the erroneous behavior, but for uniaxial tension the stress does not reduce exactly to zero. In the model M4 the erroneous behavior has been limited by introducing the positive volumetric boundary which ensures that the stress reduces to zero but causes an unrealistic lateral behavior for uniaxial tension. As can be seen in Fig. 2b, the lateral strains do not exactly reduce to zero. To eliminate this inaccurate behavior Bažant and Caner (2005) developed a new version of microplane model called M5 in which they coupled in series a kinematically constrained microplane system, such as the microplane model M4, with a statically constrained microplane system simulating solely the cohesive tensile fracture.

An alternative approach has been proposed (see also Bažant et al., 2004) in which for dominant tensile failure and after the peak load a no-split of the normal component is imposed for all the microplanes. The positive volumetric boundary has been removed, and a "transition function" φ depending on the maximum principal stress σ_I, the volumetric strain ϵ_v and the minimum principal strain ϵ_{III} has been introduced

$$f(\sigma_I) = \begin{cases} \sin\left(\frac{\pi}{2}\cdot\min\left(\frac{\langle\sigma_1+Ek_1k_6c_{27}\rangle}{Ek_1k_6c_{13}};1\right)\right) & \text{if } \epsilon_{III} > -k_1k_6c_{19}, \\ 0 & \text{if } \epsilon_{III} \leqslant -k_1k_6c_{19}. \end{cases}$$

$$\varphi(\epsilon_v,\sigma_I) = 1 - \exp\left(-f(\sigma_I)\cdot\frac{\langle\epsilon_v - k_1k_6c_{14}\rangle}{k_1k_6c_{14}}c_{15}\right) \tag{10}$$

where the fixed (c_{13}, c_{14}, c_{15}, c_{19}, c_{27}) and adjustable (k_1, k_6) parameters are defined in the Appendix I. Thus, the normal stress is now calculated through the following formula

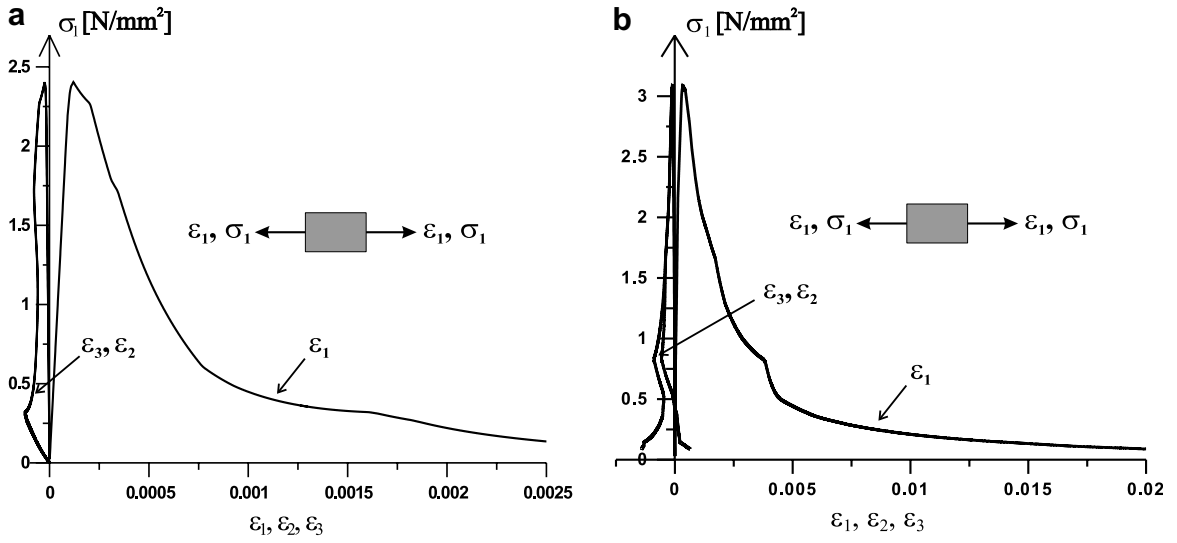

Fig. 2. Stress–strain curves for uniaxial tensile: (a) using the transition function; (b) original M4 formulation.

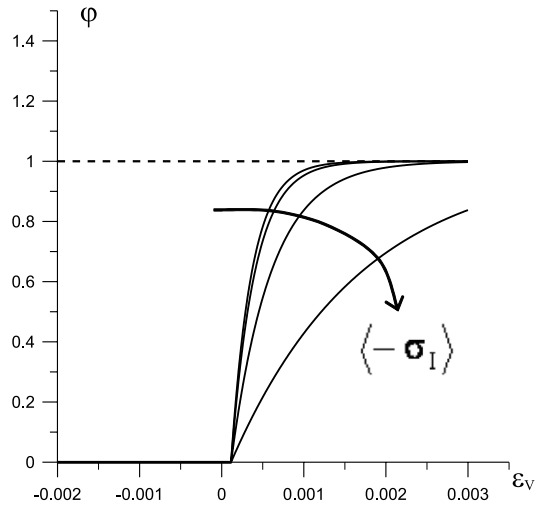

Fig. 3. The transition-function vs the volumetric strain for different values of the maximum principal stress.

$$\sigma_N = \varphi \sigma_N^{\text{no split}} + (1-\varphi)\sigma_N^{\text{split}} \tag{11}$$

where $\sigma_N^{\text{no split}}$ and σ_N^{split} are the normal microplane stresses obtained from the no-split formulation and from formulation with the split of normal microplane component, respectively, as follows:

$$\begin{aligned} \sigma_N^{\text{no split}} &= \sigma_N^{\text{no split, pre}} + E_N \Delta\epsilon_N \leqslant F_N(\epsilon_N) \\ \sigma_N^{\text{split}} &= \sigma_D + \sigma_V \leqslant F_N(\epsilon_N) \end{aligned} \tag{12}$$

where $F_N(\epsilon_N)$ is the normal boundary (see Appendix I), $E_N = E/(1-2v)$ is the normal stiffness, and $\Delta\epsilon_N$ is the normal strain increment. The transition function $\varphi(\epsilon_v, \sigma_I)$, plotted in Fig. 3 for different values of the maximum principal stress, is equal to 0 as long as a dominant tensile failure is achieved (for example in a uniaxial tensile test, the transition function is set to zero as long as the post-peak branch is not reached). At that point the function $\varphi(\epsilon_v, \sigma_I)$ grows to the unit value, such that a skip to the formulation with no-split of the normal components for all the microplanes is applied. Calculating the normal stress through Eq. (11), we obtain for

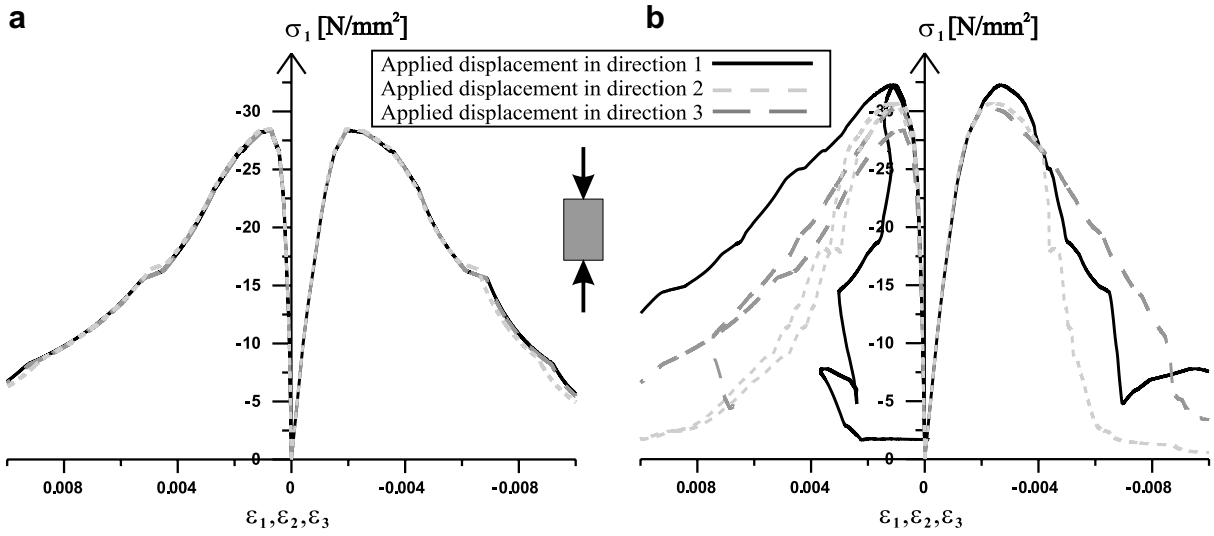

Fig. 4. Stress–strain curves for uniaxial compression with different direction of applied displacement: (a) using Alt-I; (b) using Alt-II.

uniaxial tension the macroscopic stress–strain curves plotted in Fig. 2a, where the erroneous behavior does not show up.

In the original microplane model M4 (Bažant et al., 2000), the shear stress at the boundary $\sigma_{\mathrm{T}}^{\mathrm{b}} = F_{\mathrm{T}}(\sigma_{\mathrm{N}})$ and the elastic shear stresses $\sigma_{\mathrm{L}}^{\mathrm{e}} = \sigma_{\mathrm{L}}^{\mathrm{pre}} + E_{\mathrm{T}}\Delta\epsilon_{\mathrm{L}}$ and $\sigma_{\mathrm{M}}^{\mathrm{e}} = \sigma_{\mathrm{M}}^{\mathrm{pre}} + E_{\mathrm{T}}\Delta\epsilon_{\mathrm{M}}$ are computed first, and the shear stress can then be calculated in two alternative ways: Alt-I – calculate the shear stresses in the $\vec{l}$ and $\vec{m}$ directions imposing independently the shear boundary on the two components as $\sigma_{\mathrm{L}} = \mathrm{Sign}(\sigma_{\mathrm{L}}^{\mathrm{e}})\min(|\sigma_{\mathrm{T}}^{\mathrm{b}}|, |\sigma_{\mathrm{L}}^{\mathrm{e}}|)$ and $\sigma_{\mathrm{M}} = \mathrm{Sign}(\sigma_{\mathrm{M}}^{\mathrm{e}})\min(|\sigma_{\mathrm{T}}^{\mathrm{b}}|, |\sigma_{\mathrm{M}}^{\mathrm{e}}|)$; Alt-II – calculate the resultant of the elastic shear stresses as $\sigma_{\mathrm{T}}^{\mathrm{e}R} = \sqrt{(\sigma_{\mathrm{L}}^{\mathrm{e}})^2 + (\sigma_{\mathrm{M}}^{\mathrm{e}})^2}$ and determine the unit vector in the direction of the resultant, $\vec{R} = (\sigma_{\mathrm{L}}^{\mathrm{e}}, \sigma_{\mathrm{M}}^{\mathrm{e}})/\sigma_{\mathrm{T}}^{\mathrm{e}R}$, impose the shear boundary on the resultant of the elastic shear stresses, $\sigma_{\mathrm{T}}^{R} = \min(\sigma_{\mathrm{T}}^{\mathrm{b}}, \sigma_{\mathrm{T}}^{\mathrm{e}R})$, and compute the shear stresses as $(\sigma_{\mathrm{L}}, \sigma_{\mathrm{M}}) = \sigma_{\mathrm{T}}^{R}\vec{R}$. The user can choose alternatively Alt-I or Alt-II (Bažant et al., 2000). However it is worth noting that Alt-I leads to a prediction of different stress–strain curves when the displacement is applied for different directions. In Fig. 4a the stress–strain curves for uniaxial compression simulations are plotted for applied displacement in three different orthogonal directions. Looking at the curves in Fig. 4a, it is clear how the model response depends on the direction of the applied displacement. Using Alt-II, however, this drawback disappears, as can be seen in Fig. 4b, where all the curves for the same simulations of the Fig. 4a coincide. This last feature was also presented in Bažant et al. (2004).

4. Symmetric over-nonlocal microplane Model M4

The microplane model differs from a classical tensorial plasticity or continuum damage model because the stress–strain boundaries, which define the inelastic strain, depend on the total strain only. This suggests a nonlocal generalization in which the stress–strain boundaries are evaluated from the nonlocal total strains (instead of being evaluated from the local total strain, with the nonlocal averaging postponed until after the inelastic strains have been evaluated). Based on these considerations, Bažant and Di Luzio (2004) proposed a new kind of nonlocal formulation in which the elastic stress increments are local and the boundaries in Eq. (9) are modified as follows:

$$\sigma_{\mathrm{N}} \leqslant F_{\mathrm{N}}(\widehat{\epsilon_{\mathrm{N}}}), \quad F_{\mathrm{D}}^{-}(\widehat{\epsilon_{\mathrm{D}}}) \leqslant \sigma_{\mathrm{D}} \leqslant F_{\mathrm{D}}^{+}(\widehat{\epsilon_{\mathrm{D}}}), \quad |\sigma_{\mathrm{T}}| \leqslant F_{\mathrm{T}}(\sigma_{\mathrm{N}}, \sigma_{\mathrm{V}}, \widehat{\epsilon_{\mathrm{I}}}). \tag{13}$$

For the sake of generality, the arguments in these conditions are considered as over-nonlocal

$$\widehat{\epsilon}_{\mathrm{V}} = \widehat{\epsilon}_{kk}/3, \quad \widehat{\epsilon}_{\mathrm{N}} = N_{ij}\widehat{\epsilon}_{ij}, \quad \widehat{\epsilon}_{\mathrm{D}} = \widehat{\epsilon}_{\mathrm{N}} - \widehat{\epsilon}_{\mathrm{V}}, \quad \widehat{\epsilon}_{\mathrm{M}} = M_{ij}\widehat{\epsilon}_{ij}, \quad \widehat{\epsilon}_{\mathrm{L}} = L_{ij}\widehat{\epsilon}_{ij}, \tag{14}$$

where ϵ_{ij} are the Cartesian components of $\boldsymbol{\epsilon}$, and $\widehat{\epsilon}_{ij}$ are the over-nonlocal strains defined as

$$\hat{\epsilon}_{ij} = \int_{\mathrm{V}} \alpha_m^{**}(\mathbf{x}, \boldsymbol{\xi})\epsilon_{ij}(\boldsymbol{\xi})\,\mathrm{d}V(\boldsymbol{\xi}) \tag{15}$$

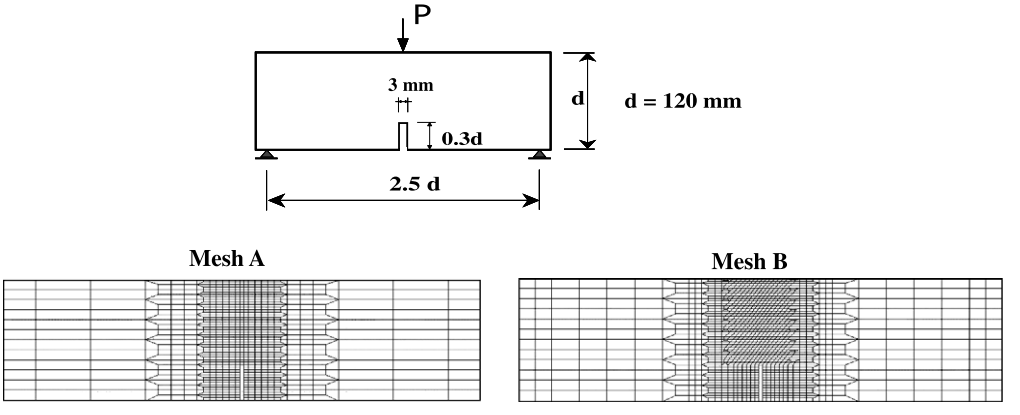

Fig. 5. Three-point bending test: geometry and used meshes for the analysis of the directional bias meshes.

in which the weight function $\alpha_m^{**}(\mathbf{x}, \boldsymbol{\xi})$ for a symmetric over-nonlocal formulation is defined in Eq. (8). The standard symmetric nonlocality is the special case for $m = 1$. It is crucial to recognize that the elastic strains on the microplane (as well as any hardening inelastic strains) must depend only on the local strain, or else one would engender zero energy instability modes. This means that in every constitutive law in which the softening law depends on the total strains objectivity can be reached by making the softening function dependent on the nonlocal strains. For the nonlocal generalization of microplane model M4, only using $m > 1$ is a realistic description of the fracturing process achieved (Bažant and Di Luzio, 2004). It was also shown that the fracturing strain localizes into a finite length, independently of the number of elements, only if m is larger than 1. On the other hand, if the classical nonlocal model ($m = 1$) is adopted, the fracturing strain tends to localize into one element even if the global response is correct (i.e., objective) in terms of the stress-displacement curve.

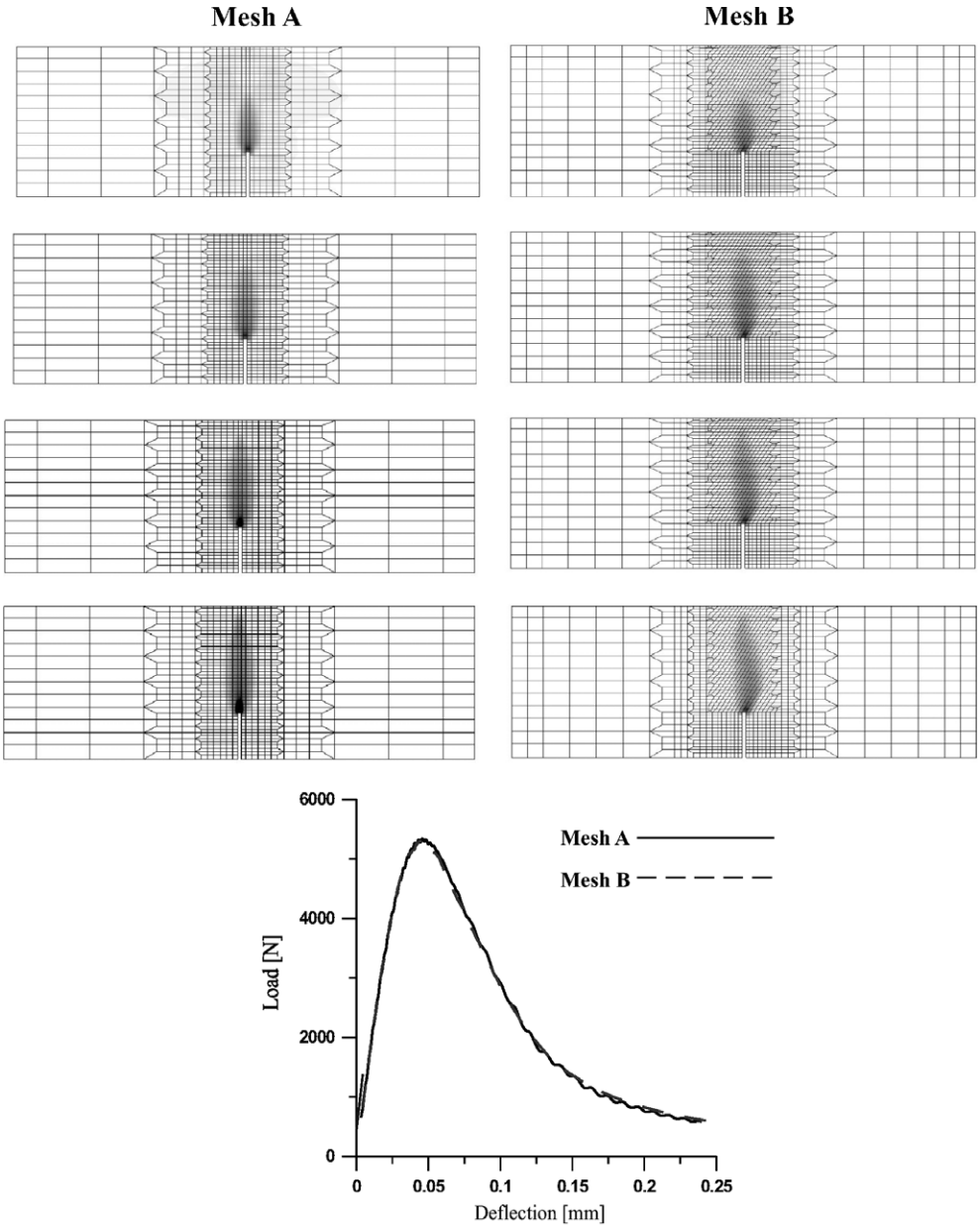

Fig. 6. Three-point bending test: maximum principal strain evolution using two different meshes.

A reliable constitutive model should be able to simulate a fracture propagation direction at an angle to the mesh line. One important feature of the over-nonlocal formulation compared with the standard nonlocal formulation, i.e. $m = 1$, is that it does not suffer from the directional mesh bias. The phenomenon is studied by simulating a three-point bending test using the specimen geometry, boundary conditions and the meshes shown in Fig. 5. The lines of the slanted mesh are inclined by about 30° respect to the vertical. Fig. 6 presents the load-displacement curves and the evolution of the maximum principal strain for both meshes with lines which are slanted and parallel with respect to the fracture propagation direction. One can see that both meshes give practically the same load-displacement curve, and the same is true for fracture propagation at different load levels (Fig. 6). However, using a nonlocal microplane M4 with $m = 1$, the numerical solution exhibits a pronounced mesh bias for the fracture propagation (Fig. 7). This phenomenon can be explained by the fact that the standard nonlocal model ($m = 1$) leads to a localization in one single element, as demonstrated by Bažant and Di Luzio (2004). Thus the standard nonlocal formulation (with $m = 1$) is much more sensitive to the mesh bias than the over-nonlocal formulation.

Another fundamental issue of the proposed symmetric over-nonlocal M4 model is revealed by considering the analysis of notched specimens loaded for a three-point-bending test. The failure initiation is located at the notch tip: damage starts to grow from the notch and propagates into the bulk of the solid. In the classical nonlocal average (non-symmetric weight function) the stress and strain fields are significantly altered in the vicinity of the boundaries. This is due to the nonlocal average integral type of the formulation: the nonlocal variable which controls the damage initiation is calculated ahead the crack tip and not at the crack tip as it is expected (the same observation has been shown by Simone (2003) for a nonlocal damage model). The maximum of the nonlocal variable which controls the softening evolution is at a certain distance from the crack tip and this distance is proportional to the characteristic length of the nonlocal model. To demonstrate this peculiar behavior of a nonlocal model, the results in terms of the strain and stress profiles along the ligament of a

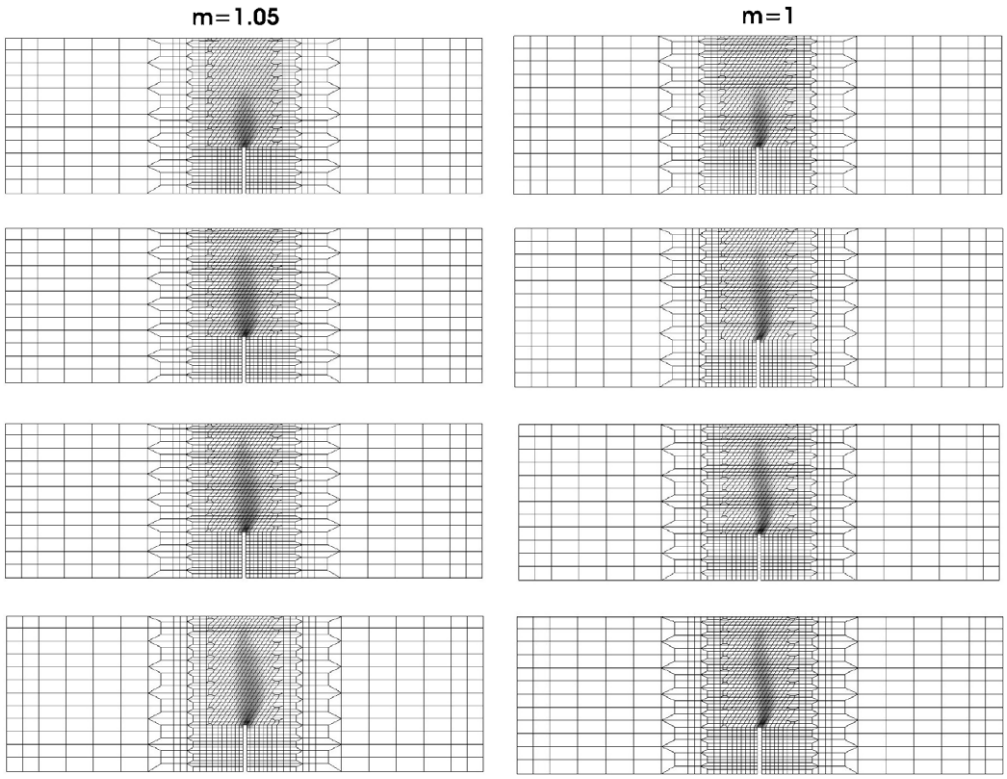

Fig. 7. Three-point bending test: maximum principal strain evolution for a slanted mesh using the over-nonlocal formulation ($m = 1.05$) on the left side and using the standard nonlocal formulation ($m = 1$) on the right side.

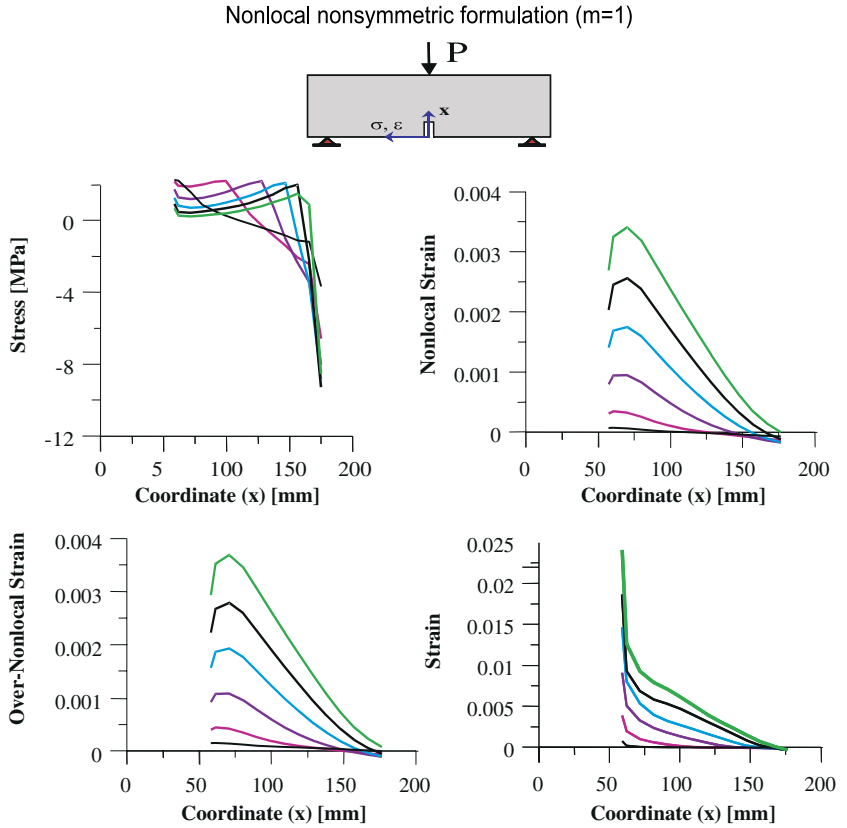

Fig. 8. Three-point bending test: stress and strain profiles along the ligament for different value of the imposed deflection using the standard nonsymmetric nonlocal formulation ($m = 1$).

specimen under a three-point-bending loading conditions are analyzed. In Fig. 8 the evolution of the stress and strains along the ligament is shown when the classical standard nonlocal average (non-symmetric weight function with $m = 1$) is used. It is evident that the calculated nonlocal strain has a non-realistic shape along the ligament, and consequently the stress field is also altered and the stress at the tip always has a larger value than its vicinity. This strange behavior cannot be eliminated using the over-nonlocal formulation, as shown in Fig. 9. On the contrary, the over-nonlocal formulation emphasizes the aforesaid problem. Therefore, the only way to obtain a reasonable field of the nonlocal quantity in the vicinity of the notch tip is to modify the averaging operation when it approaches the boundary of the body domain. Adopting the symmetric weight function presented in the previous paragraph and a small value for the over-nonlocal parameter m, a correct reproduction of the strain and stress fields can be obtained, as presented in Fig. 10. Since a large value for the over-nonlocal parameter m can also alter the correct calculation of the over-nonlocal quantity (Fig. 11), a value just slightly larger than unity (e.g. $1 < m \leqslant 1.1$) for the parameter m must be used in the numerical applications.

5. Numerical simulation of fracture tests

Without a nonlocal formulation (in general without a regularization technique) the finite-element codes with strain softening exhibit unacceptable spurious mesh sensitivity. To demonstrate the capability of the present over-nonlocal symmetric formulation of microplane model M4, the finite element simulations of three different tests in which the crack has either a straight or a curved path are presented. Monotonic loading and small strains and rotations are assumed. Three-dimensional 8-node brick elements and explicit time integra-

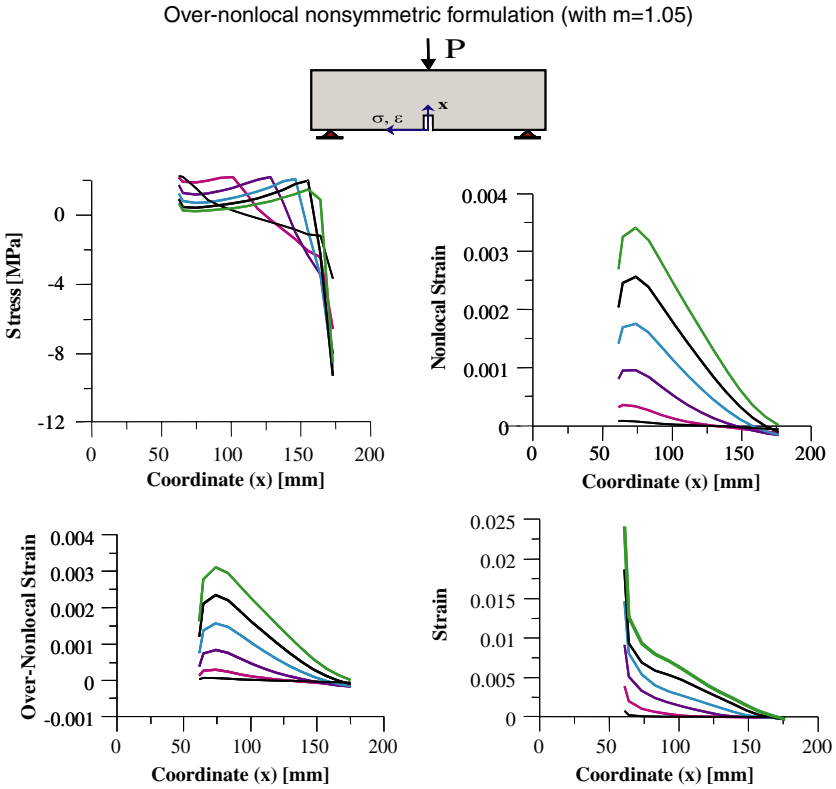

Fig. 9. Three-point bending test: stress and strain profiles along the ligament for different value of the imposed deflection using the nonsymmetric over-nonlocal formulation with $m = 1.05$.

tion are used in the calculations. The capability of the proposed model in the simulation of mode-I fracture propagation has been already shown in a recent conference paper (Di Luzio, 2004).

The size of the process zone and the macroscopic fracture energy depend on both the values of parameters m and l (characteristic length). Because the parameter m must be kept relatively small, as previously shown, it can be considered as a constant. Therefore, the desired fracture energy is achieved by changing only the characteristic length l, if the local fracture energy is kept constant.

5.1. Four-point-bending

Recently an experimental investigation on four-point-bending tests with sharp notches of different length was conducted by CTG-Italcementi Group (Rambaldini, 1999). The concrete specimens used, with a depth of 150 mm, had three different notch lengths: 30, 52.5 and 75 mm (Fig. 12 shows the geometry and the meshes adopted). Three specimens for each notch length were tested. The sharp notch was simulated as a trapezium with a base at the notch tip of 1 mm in accordance with the tolerance used in the concrete industry. A normal strength concrete obtained with water-cement ratio of 0.55 and maximum aggregate diameter of 15 mm has been used in the experimental investigation. The measured mechanical properties were cylindrical compressive strength, $f_c = 32$ MPa, and dynamic Young modulus, equal to 37000 MPa. The parameters of the nonlocal microplane model M4 were calibrated on the basis of the experimental results of the four-point-bending test with a notch length of 30 mm (Fig. 13a). Fig. 13b and c show the comparison between the numerical and the experimental load-deflection curves obtained for the other notch lengths 52.5 and 75 mm, respectively. This good agreement between the numerical simulations and the test results was obtained using the following values of the parameters of the nonlocal constitutive law: $E = 30{,}000$ MPa, $k_1 = 14.50 \times 10^{-5}$, $k_2 = 1000.0$, $k_3 = 10.0$, $k_4 = 150.0$, $k_5 = 1.7$, $k_6 = 0.8$, $\ell = 28$ mm and $m = 1.04$, giving $f_t = 2.55$ MPa and $G_F = 110$ Nm^{-1}.

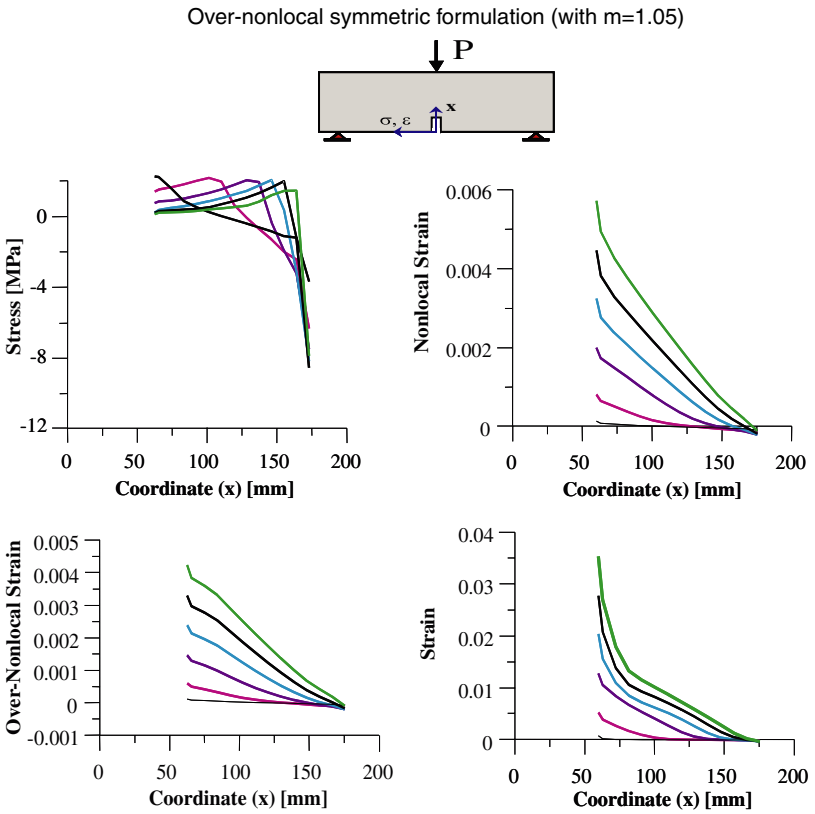

Fig. 10. Three-point bending test: stress and strain profiles along the ligament for different value of the imposed deflection using the symmetric over-nonlocal formulation with $m = 1.05$.

5.2. Four-point-shear

The second experimental investigation that has been considered is the classical single notch specimen tested by Schlangen (1993). The geometry, the loading arrangement of the specimen and the finite element mesh used are shown in Fig. 14. For this geometry the crack begins to propagate from the tip of the notch in a mixed-mode stress field. After that, as the crack grows, it becomes almost a mode-I fracture propagation. In the past this geometry has been numerically investigated by many authors in the literature, and the best results have been obtained by micro-mechanical simulation and discrete crack approaches. Some local smeared crack approaches, such as the rotating crack model, lead to residual stresses and to incorrect crack propagation as was shown, among the others, by Jirásek and Zimmermann (1998). Other local smeared crack approaches, such as the isotropic damage model, lead to incorrect crack propagation as was recently demonstrated by Grassl and Jirásek (2004). As shown in Fig. 15, failure in the numerical simulations as well as in the experiments is characterized by a macroscopic crack which propagates from the notches in an inclined direction. The calculated crack pattern (shown through the maximum principal strain on the deformed mesh in Fig. 15) is reasonably in agreement with the pattern observed in the experiments. The finite elements located at the crack tip reduce their distortion during the evolution of the test, which means that the mixed-mode fracture observed at crack initiation degenerates to a mode-I fracture at failure, characterized by finite elements deformed mainly in the horizontal direction (Fig. 15). The calculated and the experimentally measured total load versus crack-mouth-opening-displacement (CMOD) and total load versus crack-mouth-sliding-displacement (CMSD) are plotted in Fig. 16a and b, respectively. The agreement between the numerical and the experimental results is quite satisfactory. The following values of the parameters of the nonlocal constitutive law were used in finite element analysis: $E = 30{,}000$ MPa, $k_1 = 20.0 \times 10^{-5}$, $k_2 = 1000.0$, $k_3 = 10.0$, $k_4 = 150.0$, $k_5 = 1.0$, $k_6 = 0.95$, $\ell = 20$ mm and $m = 1.05$.

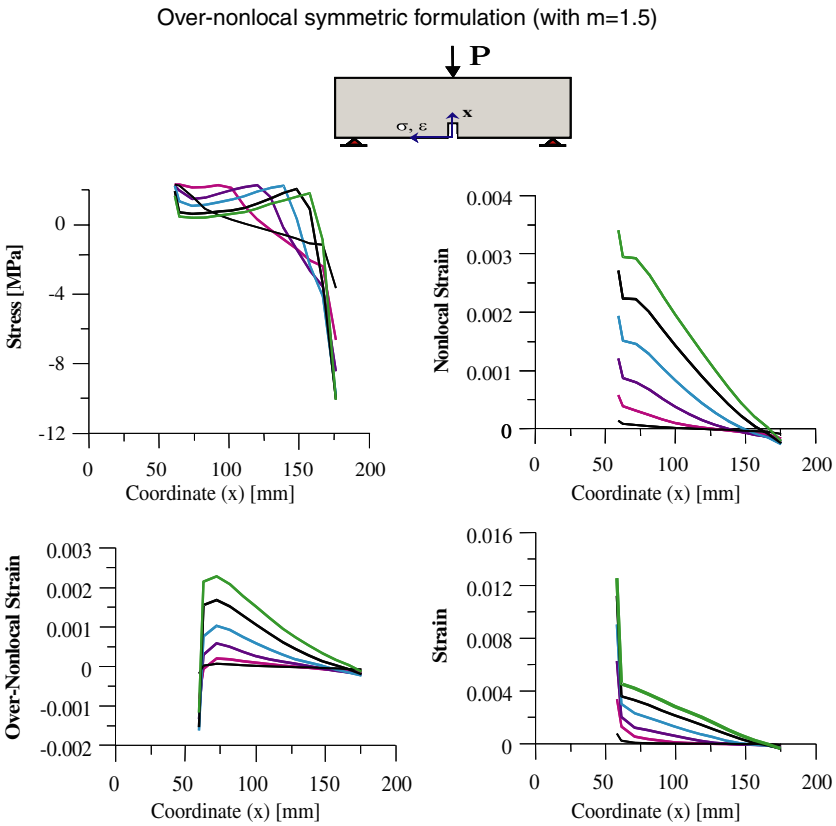

Fig. 11. Three-point bending test: stress and strain profiles along the ligament for different value of the imposed deflection using the nonsymmetric over-nonlocal formulation with $m = 1.5$.

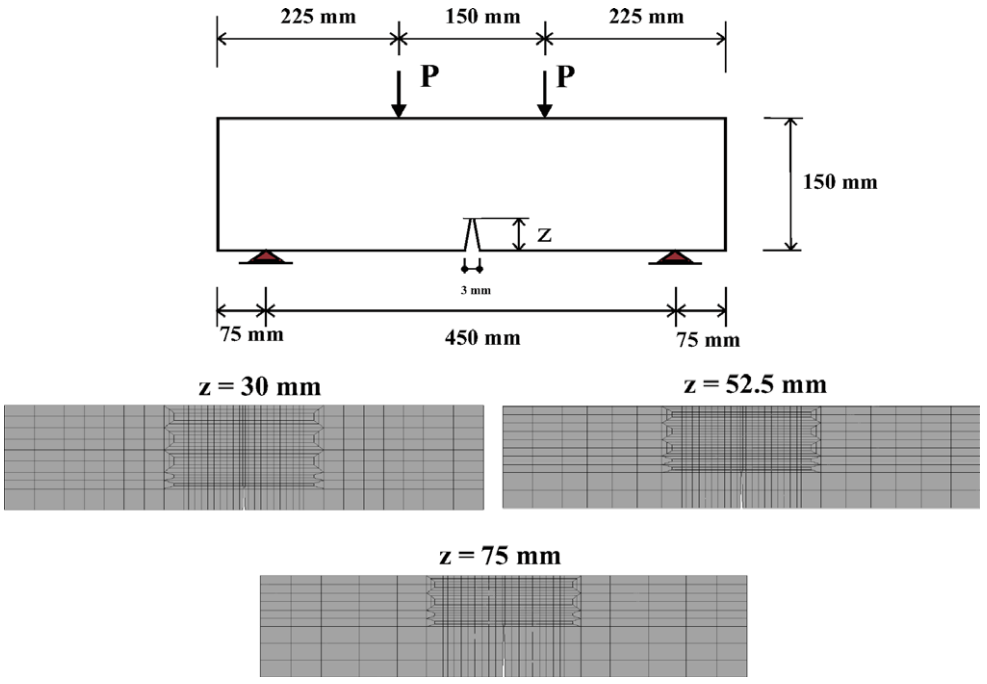

Fig. 12. Four-point-bending geometry and corresponding meshes for three different notch lengths.

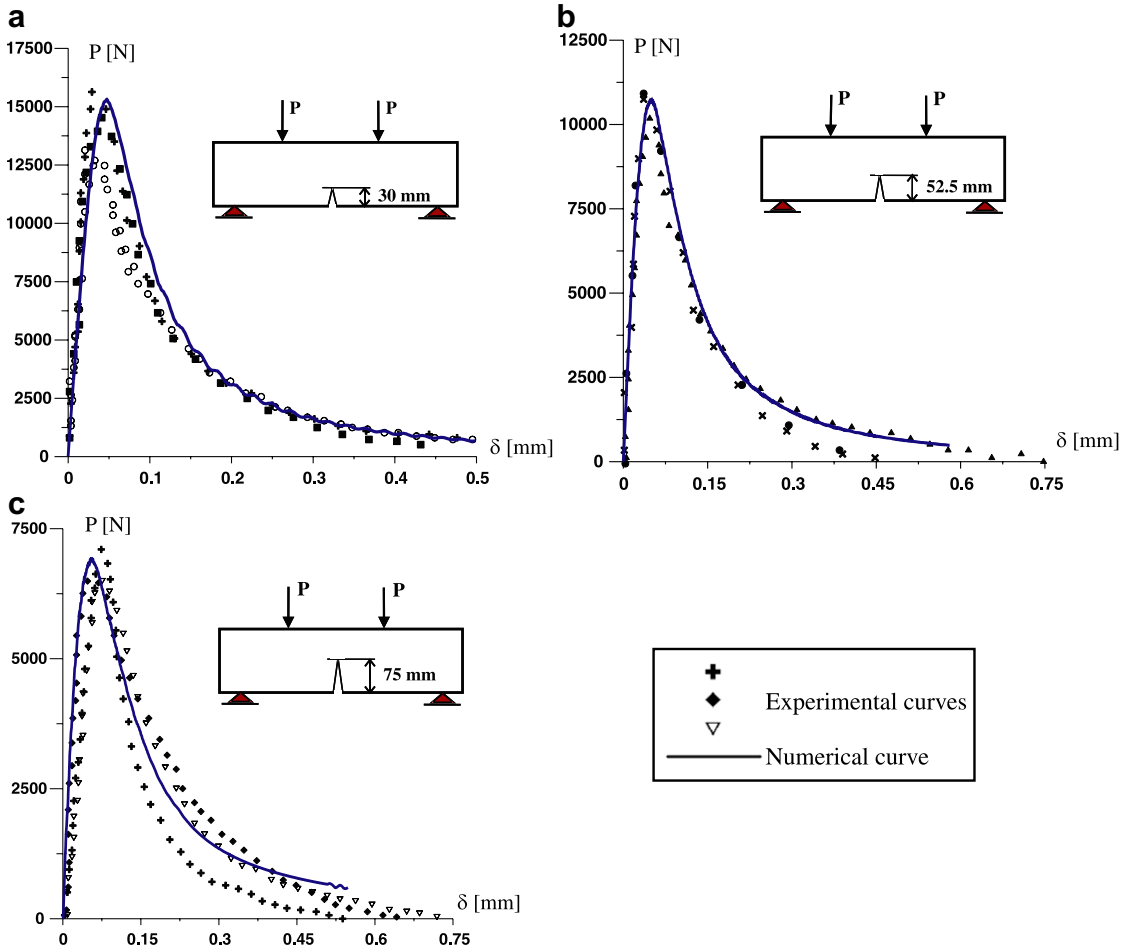

Fig. 13. Comparison between the numerical and the experimental load–deflection curves of the specimens with a notch length of 30 mm (a), 52.5 mm (b), and 75 mm (c).

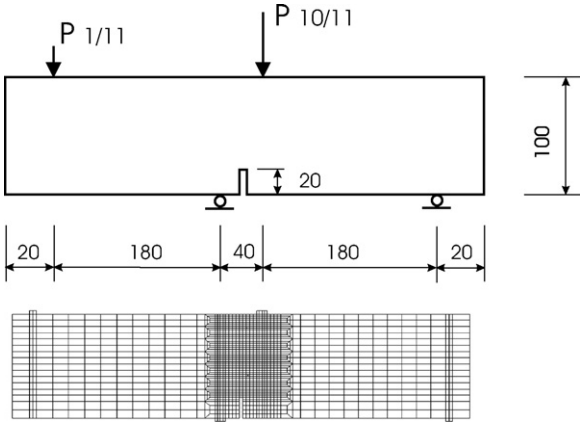

Fig. 14. Single-edge-notched beam subject to antisymmetric four-point shear loading: geometry and the corresponding mesh.

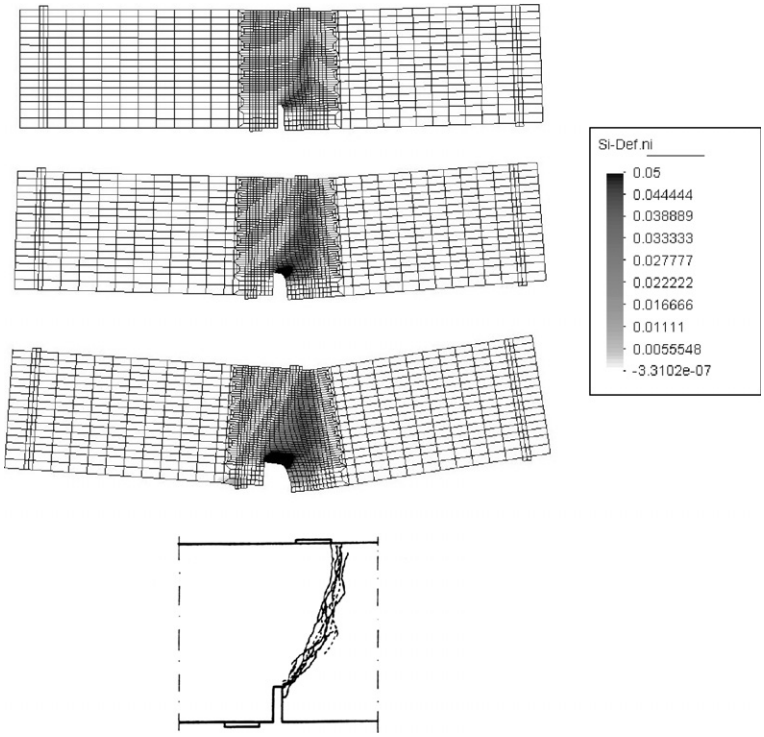

Fig. 15. Single-edge-notched beam subject to antisymmetric four-point shear loading: crack propagation (based on maximum principal strain on the deformed mesh).

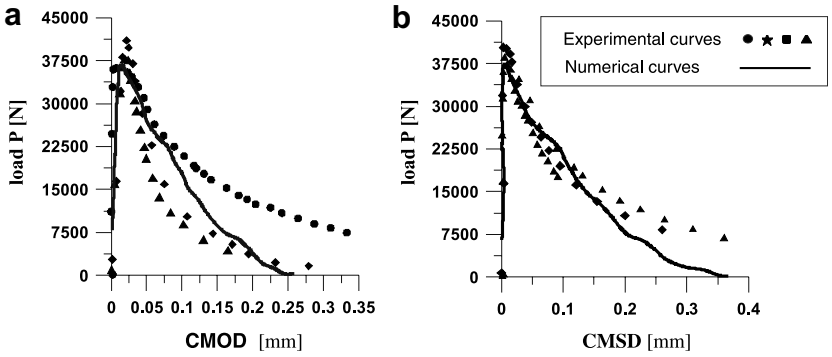

Fig. 16. Single-edge-notched beam subject to antisymmetric four-point shear loading: (a) total load vs CMOD; (b) total load vs CMSD.

5.3. Tensile test with constant shear load

The third example concerns the double-edge-notched (DEN) specimen experimentally tested by Nooru-Mohamend (1992). Shown in Fig. 17a is the configuration of the mixed-mode plain concrete fracture test, in which a special loading frame allows for the analysis of various loading paths combining shear and tension. In order to reproduce the very stiff frame to which the specimen is glued, the nodes of the finite element model located at the top edge are forced to remain horizontal and the nodes located at the upper part of the left edge are forced to remain vertical. All nodes located at the bottom edge and the lower part of the right edge are fixed. Our attention is focused on the largest specimen, square plates 200×200 mm and 50 mm of thickness, loaded according to path 4. For this path 4 the shear load P_s is kept constant, with values of $P_s = 5$ kN,

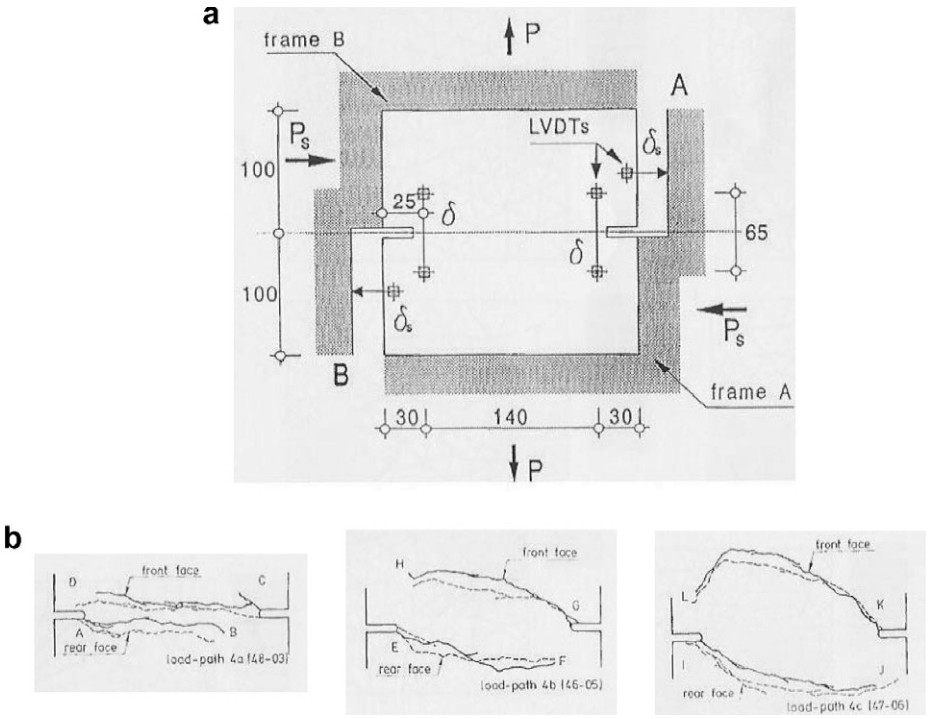

Fig. 17. DEN specimen of Nooru-Mohamend tests: (a) experimental set-up; (b) observed crack patterns (taken from Nooru-Mohamend, 1992).

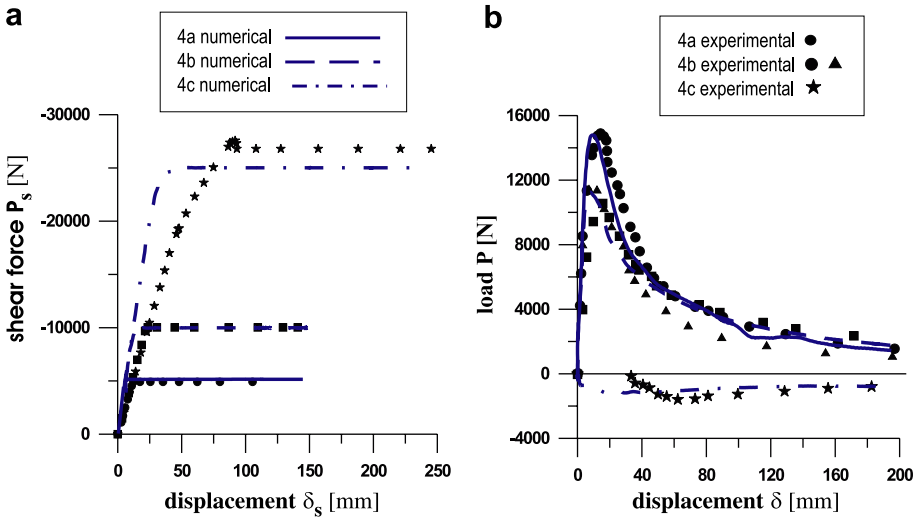

Fig. 18. Nooru-Mohamend test load-path 4. Calculated and measured load-displacement curves: (a) tensile load versus the average of the normal displacement; (b) shear force versus transversal displacement δ_s.

$P_s = 10$ kN and $P_s = P_s^{max} = 27.5$ kN (maximum shear force) for the paths 4a, 4b and 4c, respectively. The shear force is applied first with the zero normal force. After the shear force has reached the prescribed value, it is kept constant and a normal displacement is applied, giving a non-zero reaction in the normal direction. The material parameters are identified by the fit of the experimental data ($k_1 = 18.0 \times 10^{-5}$, $k_2 = 1000.0$, $k_3 = 10.0$, $k_4 = 150.0$, $k_5 = 1.55$, $k_6 = 0.67$, $\ell = 24$ mm and $m = 1.04$), resulting in a tensile strength of 2.75 MPa and a compressive strength of 46 MPa.

The agreement between the experimental and the numerical load-displacement curves, plotted in Fig. 18, is satisfactory. For loading paths 4a and 4b, where the shear response is linear, the normal load-displacement curves are in good agreement. For loading path 4c, the maximum shear force measured in the test is 27.5 kN and in the simulation is 25.1 kN showing a certain discrepancy between the experimental and the numerical results. The numerical calculation correctly provides a compressive normal reaction force, which however has a maximum value of 1.1 kN compared to 1.5 kN measured in the test. One can also observe that the measured displacement δ_s exceeds the computed one. The underestimation of the shear displacement δ_s has been also observed in other numerical simulations of this test (Di Prisco et al., 2000). It can be explained by the occurrence of some inelastic deformation between the specimen and the loading platens.

As shown in Fig. 17b, the failure is characterized by two macroscopic cracks which propagate from the notches in an inclined direction. Increasing the applied shear force, the trajectory of the failure cracks shows an increase in curvature (Fig. 17b). The evolution of the cracks obtained in the finite element simulations is shown in Figs. 19–21 for the three loading paths 4a, 4b and 4c, respectively. It is clear that for all loading paths the numerical cracks' trajectories are in good agreement with the experimental ones (17b). For path 4a, the

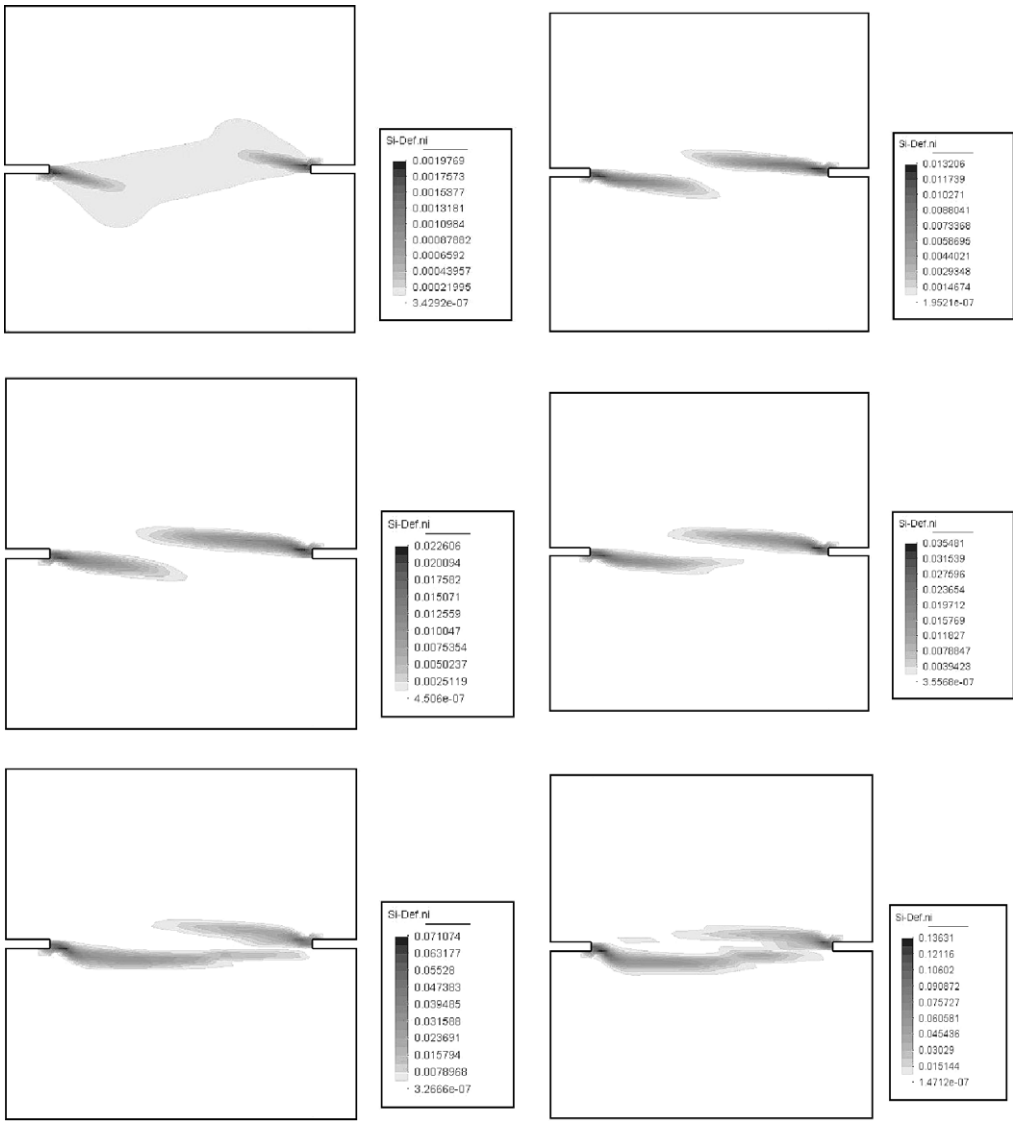

Fig. 19. Nooru-Mohamend test load-path 4a: evolution of the maximum principal strain.

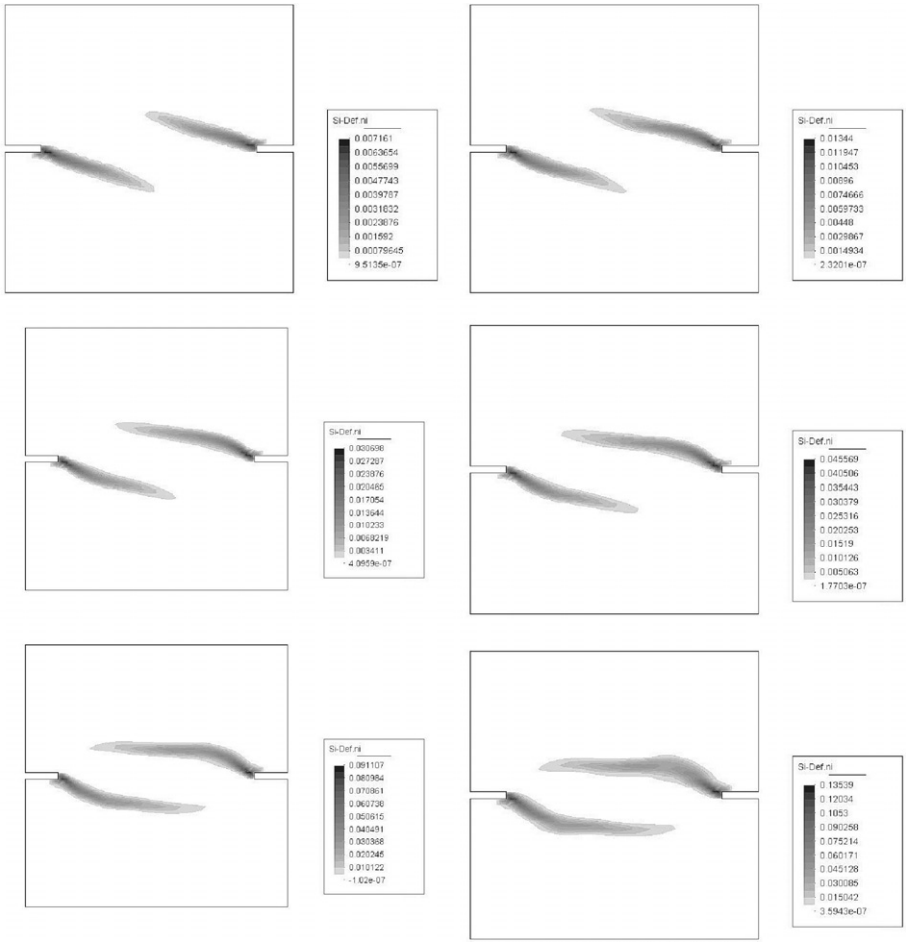

Fig. 20. Nooru-Mohamend test load-path 4b: evolution of the maximum principal strain.

cracks' propagation is almost horizontal (Fig. 19), while for path 4b, the cracks show a more curved trajectory (Fig. 20). For path 4c, the cracks are farther away and highly curved.

6. Concluding remarks

The presented microplane model M4 is a macroscopic three-dimensional model for concrete based on the kinematic constraint approach which leads to a pathological model response for dominant tensile load. The main reason of the pathological behavior is the split of the normal microplane component into the volumetric and deviatoric part. The model is improved by the transition to a microplane model without the split of the normal microplane component for dominant tensile load in the nonlinear regime. The transition is controlled by a function which depends on the total volumetric strain and the maximum principal stress. The reason is that for the localization of tensile damage the stress and the strain on the microplanes are better controlled without the split of the normal components. It is demonstrated that the new microplane model M4 predicts physically correct results.

The symmetric over-nonlocal microplane model M4 is a constitutive law capable of predicting the fracture propagation ensuring the objectiveness of the numerical results. Moreover, it is able to give a physically meaningful reproduction of the nonlocal variable, and consequently of the stress and strain fields in the vicinity of a boundary, which typically does not happen in classical non-symmetric non-local formulation. It has been also demonstrated that the over-nonlocal parameter m must have a value a little bit bigger than unity

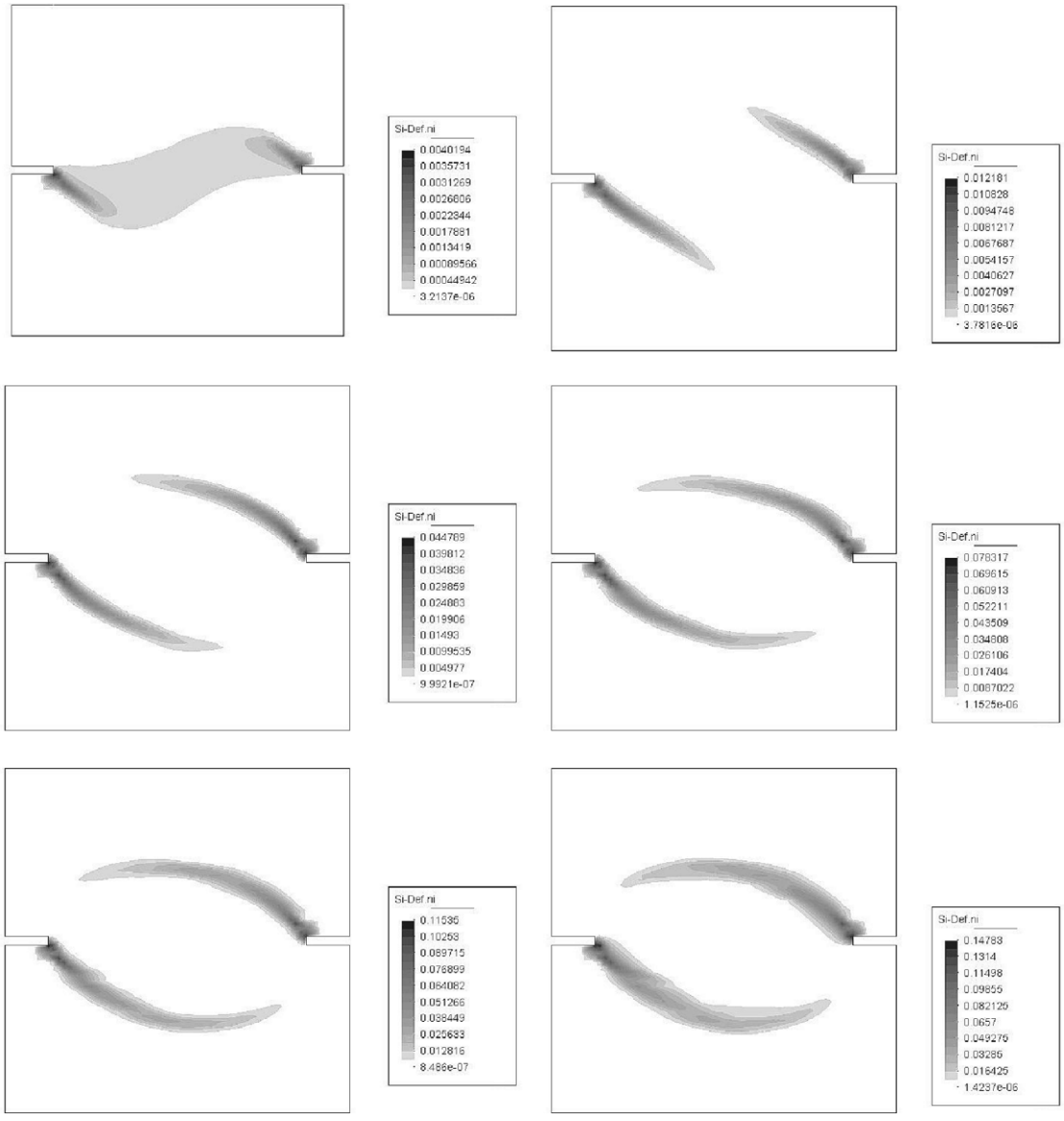

Fig. 21. Nooru-Mohamend test load-path 4c: evolution of the maximum principal strain.

($1 < m \leqslant 1.1$). The proposed model has been applied for the simulation of standard fracture tests achieving satisfactory agreement between the numerical and the experimental results. The symmetric over-nonlocal microplane model M4 correctly predicts both structural response and crack pattern for all investigated geometries characterized by both mixed-mode and mode-I fracture propagation.

Acknowledgement

The authors acknowledge Gianluca Merlo for his help in the numerical development of the model.

Appendix I. Microplane model M4

The microplane model M4, formulated and tested by Bažant and coworkers (Bažant et al., 2000; Caner and Bažant, 2000), has the inelastic behavior characterized on the microplane level by the so-called stress–strain

boundaries, which may be regarded as strain-dependent yield limits and exhibit strain softening (Bažant et al., 1996). Within the boundaries, the response is incrementally elastic, although the elastic moduli may undergo progressive degradation as a result of damage. Exceeding the boundary stress is never allowed. Travel along the boundary is permitted only if the strain increment is of the same sign as the total stress. Otherwise elastic unloading occurs. Experience with data fitting has shown that each microplane stress component (normal, volumetric and deviatoric) can be assumed to depend only on its conjugate strain, i.e., the boundary stress σ_N depends only on ϵ_N, σ_V only on ϵ_V, and σ_D only on ϵ_D. Only in the shear boundary, which describes frictional interaction between two different stress components, do the normal stress and the shear stress interact. The material parameters are divided into the fixed (or constant) parameters, which are denoted as c_i and may be taken the same for all concretes, and the free parameters, which are denoted as k_i and reflect the differences among different concretes. They are dimensionless, except for the Young's elastic modulus E. The original formulation of the microplane model M4 (Bažant et al., 2000) has been modified as presented in the Section 3 by introducing a no-split of the normal component for the dominant tensile failure (removing the tensile volumetric boundary) and by imposing the shear boundary on the shear stress resultant instead of on the single shear components individually. Moreover, to improve the prediction performance of the microplane model M4, two free parameters were added. These new free parameters are k_5 and k_6. The parameter k_5 can modify the slope of the softening branch of the uniaxial tensile or compression stress–strain curve. The parameter k_6 is able to set a different ratio between the tensile and the compression strength.

Normal stress boundaries. The tensile normal boundary is given as

$$F_{\mathrm{N}}(\epsilon_{\mathrm{N}}) = Ek_1k_6c_1 \exp\left(-\frac{\langle \epsilon_{\mathrm{N}} - k_1k_6c_1c_2\rangle}{k_1k_5k_6c_3 + \langle -c_4(\sigma_{\mathrm{v}}/E_{\mathrm{v}})\rangle}\right), \tag{16}$$

The Macaulay brackets, defined as $\langle x\rangle = \mathrm{Max}(x; 0)$, are used here and in several subsequent formulas to define horizontal segments of the boundaries, representing yield limits. In addition, the closing of cracks after tensile unloading needs to be represented by a crack closing boundary, defined simply as $\sigma^b_{\mathrm{N}} = 0$ for $\epsilon_{\mathrm{N}} > 0$; it prevents entry into the quadrant of positive ϵ_{N} and negative σ_{N} on the microplane level (however, in terms of uniaxial stress on the macro-level, this quadrant can be entered because of microplane interactions and deviatoric stresses).

Transition function. As explained in Section 3, a transition function has been introduced because it allows the microplane model with the split of the normal component to be coupled with a model with no-split of the normal component; the later of which controls the response only for dominant tensile failure load (in nonlinear regime). The transition function φ, which depends on the maximum principal stress σ_{I}, the volumetric strain ϵ_{v} and the minimum principal strain ϵ_{III}, is given by Eq. (10). Thus, the normal stress is now calculated through the Eqs. (11) and (12), as previously presented.

Deviatoric boundaries. The compressive and the tensile deviatoric boundary have similar shapes and similar mathematical forms

$$F^{+}_{\mathrm{D}}(\epsilon_{\mathrm{D}}) = \frac{Ek_1c_5}{1 + \left(\frac{\langle \epsilon_{\mathrm{D}} - k_1c_5c_6\rangle}{k_1k_5c_7c_{20}}\right)^2} \quad \text{if } \sigma_{\mathrm{D}} > 0, \tag{17}$$

$$F^{-}_{\mathrm{D}}(-\epsilon_{\mathrm{D}}) = \frac{Ek_1c_8}{1 + \left(\frac{\langle -\epsilon_{\mathrm{D}} - k_1c_8c_9\rangle}{k_1k_5c_7}\right)^2} \quad \text{if } \sigma_{\mathrm{D}} < 0, \tag{18}$$

Frictional yield surface. The shear boundary physically represents friction. The frictional boundary is nonlinear and it is expressed as

$$F_{\mathrm{T}}(-\sigma_{\mathrm{N}}) = \frac{E_{\mathrm{T}}k_1k_2c_{10}\langle -\sigma_{\mathrm{N}} + \sigma^0_{\mathrm{N}}\rangle}{E_{\mathrm{T}}k_1k_2 + c_{10}\langle -\sigma_{\mathrm{N}} + \sigma^0_{\mathrm{N}}\rangle}\vartheta(\sigma_{\mathrm{V}}), \tag{19}$$

where

$$\sigma^0_{\mathrm{N}} = E_{\mathrm{T}}k_1k_6c_{11} \exp\left(-\frac{\langle \epsilon_{\mathrm{I}} - k_1k_6c_{21}\rangle}{c_{12}k_5}\right) \quad \text{and} \quad \vartheta(\sigma_{\mathrm{V}}) = 1 + \frac{c_{22}\mathrm{e}^{c_{23}}\xi(\sigma_{\mathrm{V}})}{1 - (1 - \mathrm{e}^{c_{23}})\xi(\sigma_{\mathrm{V}})} \tag{20}$$

with

$$\xi(\sigma_V) = \begin{cases} \min\left(\frac{\langle -\sigma_V - E_T k_1 c_{25}\rangle}{E_T k_1 c_{26}}; 1\right) & \text{if } \sigma_V > -E_T k_1 c_{24}, \\ 1 - E_T k_1 c_{28} & \text{if } \sigma_V \leqslant -E_T k_1 c_{24} \end{cases}. \tag{21}$$

Note that $\lim \sigma_{N\to\infty}\sigma_T = E_T k_1 k_2$, which represents a horizontal asymptote. The former expression involves a finite cohesion, which can be calculated by setting $\sigma_N = 0$ and $\sigma_N^0 = E_T k_1 k_6 c_{11}$. When $\epsilon_I \gg 0$, the friction boundary actually passes through the origin. The coefficient $\vartheta(\sigma_V)$, in Eqs. (20) and (21), was absent from the original model M4 and has been recently introduced in order to achieve a more realistic response when transverse compressive stresses are applied during tensile softening or when the triaxial compression under low confinement is considered (see also Ghazi et al., 2002).

Volumetric boundaries. The inelastic behavior under hydrostatic pressure is simulated by a compressive volumetric boundary in the form of a rising exponential given as

$$F_V^-(-\epsilon_V) = -E k_1 k_3 \exp\left(-\frac{\epsilon_V}{k_1 k_4}\right) \quad \text{for } \sigma_V < 0 \tag{22}$$

The positive volumetric boundary has been removed.

Unloading and stiffness degradation. For virgin loading as well as reloading of any component, the incremental (tangential) moduli are constant and equal to the initial elastic moduli E_V, E_D and E_T, with the exception of the compressive hydrostatic reloading. Unloading is assumed to occur when the work rate $\sigma\dot{\epsilon}$ (or increment $\sigma\Delta\epsilon$) becomes negative. This unloading criterion is considered separately for each microplane stress component. The following empirical rules for the incremental unloading moduli on the microplanes have been developed, with good results: for $\epsilon_V \leqslant 0$ and $\sigma_V \leqslant 0$:

$$E_V^U(-\epsilon_V, -\sigma_V) = E_V\left(\frac{c_{16}}{c_{16} - \epsilon_V} + \frac{\sigma_V}{c_{16} c_{17} E_V}\epsilon_V\right) \tag{23}$$

and for $\epsilon_V > 0$ and $\sigma_V > 0$:

$$E_V^U(\epsilon_V, \sigma_V) = \min[\sigma_V(\epsilon_V)/\epsilon_V, E_V], \quad E_D^U = (1 - c_{18})E_D + c_{18}E_D^S \tag{24}$$

where, if $\sigma_D\epsilon_D \leqslant 0 : E_D^S = E_D$; else $E_D^S = \min(\sigma_D/\epsilon_D, E_D)$.

$$E_T^U = (1 - c_{18})E_T + c_{18}E_T^S \tag{25}$$

where, if $\sigma_T\epsilon_T \leqslant 0 : E_T^S = E_T$; else $E_T^S = \min(\sigma_T/\epsilon_T, E_T)$. c_{16}, c_{17}, c_{18} are fixed dimensionless parameters, and superscript S denotes the secant modulus; c_{17} controls the unloading modulus, which is equivalent to the virgin elastic modulus for $c_{17} = 0$ and to the secant modulus for $c_{17} = 1$.

Material parameters. The default values of the adjustable parameters, denoted as k_i, and the fixed parameters, denoted as c_i, and, are assumed as:

$k_1 = 9.50 \times 10^{-5}$	$k_2 = 200.0$	$k_3 = 15.0$	$k_4 = 100.0$	$k_5 = 1.0$	$k_6 = 1.0$	
$c_1 = 0.62$	$c_2 = 0.25$	$c_3 = 1.30$	$c_4 = 2.50$	$c_5 = 2.30$	$c_6 = 2.20$	$c_7 = 200.0$
$c_8 = 4.90$	$c_9 = 0.75$	$c_{10} = 0.75$	$c_{11} = 1.30$	$c_{12} = 12.5$	$c_{13} = 0.05$	$c_{14} = 0.20$
$c_{15} = 0.01$	$c_{16} = 0.02$	$c_{17} = 0.01$	$c_{18} = 0.40$	$c_{19} = 6.70$	$c_{20} = 1.50$	$c_{21} = 0.70$
$c_{22} = 0.23$	$c_{23} = 1.00$	$c_{24} = 5.75$	$c_{25} = 3.35$	$c_{26} = 1.45$	$c_{27} = 2.00$	$c_{28} = 24.5$

The scaling of the local constitutive law M4, needed to match the stiffness and strength of different types of concrete, can be easily controlled through the adjustable parameters. The model predictions agree with the basic experimental data in uniaxial, biaxial and triaxial loading conditions as it has been demonstrated by Merlo (2003).

References

Batdorf, S.B., Budianski, B., 1949. A mathematical theory of plasticity based on the concept of slip. Technical note no. 1871. National Advisor Committee for Aeronautics, Washington D.C.

Bažant, Z.P., 1976. Instability, ductility, and size effect in strain-softening concrete. Journal of the Engineering Mechanics, ASCE 102, 331–344.

Bažant, Z.P., 1984a. Imbricate continuum and its variational derivation. Journal of Structural Engineering, ASCE 110, 1693–1712.

Bažant, Z.P., 1984b. Microplane model for strain controlled inelastic behavior. In: Desai, C.S., Gallagher, R.H. (Eds.), Mechanics of Engineering Materials. J. Wiley, London, pp. 5–59 (Chapter 3).

Bažant, Z.P., 1994. Nonlocal damage theory based on micromechanics of crack interations. Journal of Engineering Mechanics, ASCE 120, 593–617.

Bažant, Z.P., Belytschko, T., Chang, T.-P., 1984. Continuum model for strain softening. Journal of Structural Engineering, ASCE 110, 1666–1692.

Bažant, Z.P., Caner, F., 2005. Microplane model M5 with kinematic and static constraints for concrete fracture and anelasticity. I: Theory. Journal of Engineering Mechanics, ASCE 131 (1), 31–40.

Bažant, Z.P., Caner, F.C., Cedolin, L., Cusatis, G., Di Luzio, G. 2004. Fracturing material models based on micromechanical concepts: recent advances. In: Li, V.C., Leung, C.K.Y., Willam, K.J., Billington S.L. (Eds.), Proceedings of the Fracture Mechanics of Concrete and Concrete Structures – FraMCoS-5, Vail Colorado, pp. 83–89.

Bažant, Z.P., Caner, F., Carol, I., Adley, M., Akers, S.A., 2000. Microplane model M4 for concrete. I: Formulation with work-conjugate deviatoric stress. Journal of Engineering Mechanics, ASCE 126, 944–953.

Bažant, Z.P., Chang, T.-P., 1984. Instability of nonlocal continuum and strain averaging. Journal of Engineering Mechanics, ASCE 110, 1441–1450.

Bažant, Z.P., Di Luzio, G., 2004. Nonlocal microplane model with strain-softening yield limits. International Journal of Solids and Structure 41 (24-25), 7209–7240.

Bažant, Z.P., Gambarova, P., 1984. Crack shear in concrete: crack band microplane model. Journal of Engineering Mechanics, ASCE 110, 2015–2035.

Bažant, Z.P., Jirásek, M., 1994. Localization analysis of nonlocal model based on crack interactions. Journal of Engineering Mechanics, ASCE 120, 1521–1542.

Bažant, Z.P., Lin, F.B., 1988. Nonlocal smeared cracking model for concrete fracture. Journal of Structural Engineering, ASCE 114, 2493–2510.

Bažant, Z.P., Lin, F.B., 1989. Stability against localization of softening into ellipsoids and bands: parameter study. International Journal of Solids and Structure 25, 1483–1498.

Bažant, Z.P., Oh, B.-H., 1983. Crack band theory for fracture of concrete. Material and structures, RILEM 16, 155–177.

Bažant, Z.P., Oh, B.-H., 1986. Efficient numerical integration on the surface of a sphere. Zeitschrift Fur Angewandte Mathematik Und Mechanik 66, 37–49.

Bažant, Z.P., Ožbolt, J., 1990. Nonlocal microplane model for fracture, damage and size effect in structures. Journal of Engineering Mechanics, ASCE 116, 2485–2505.

Bažant, Z.P., Planas, J., 1998. Fracture and Size Effect in Concrete and other Quasibrittle Materials. CRC Press, Boca Raton, FL.

Bažant, Z.P., Prat, P.C., 1988. Microplane model for brittle plastic material: I. Theory; and II. Verification. Journal of Engineering Mechanics, ASCE 114, 1672–1702.

Bažant, Z.P., Xiang, Y., Prat, P.C., 1996. Microplane model for concrete. I. Stress–strain boundaries and finite strain. Journal of Engineering Mechanics, ASCE 122, 245–254.

Borino, G., Failla, B., Parrinello, F., 2003. A symmetric nonlocal damage theory. International Journal of Solids and Structure 40, 3621–3645.

Caner, F., Bažant, Z.P., 2000. Microplane model M4 for concrete. II: Algorithm and calibration. Journal of Engineering Mechanics, ASCE 126, 954–961.

Di Luzio, G., 2004. Over-nonlocal microplane model M4: mode-I fracture simulations. In: Li, V.C., Leung, C.K.Y., Willam, K.J., Billington, S.L., (Eds.), Fracture Mechanics of Concrete and Concrete Structures – FraMCoS-5. Vail Colorado, pp. 287–294.

Di Luzio, G., Bažant, Z.P., 2005. Spectral analysis of localization in nonlocal and over-nonlocal materials with softening plasticity or damage. International Journal of Solids and Structure 42 (23), 6071–6100.

Di Prisco, M., Ferrara, L., Meftah, F., Pamin, J., de Borst, R., Mazars, J., Reynouard, J.M., 2000. Mixed mode fracture in plain and reinforced concrete: some results on benchmark tests. International Journal of Fracture 103, 127–148.

Eringen, A.C., 1966. A unified theory of thermomechanical materials. International Journal of Engineering Science 4, 179–202.

Ghazi, M., Attard, M.M., Foster, S.P., 2002. Modelling triaxial compression using the microplane formulation for low confinement. Computer and Structures 80, 919–934.

Grassl, P., Jirásek, M., 2004. On mesh bias of local damage models for concrete. In: Li, V.C., Leung, C.K.Y., Willam, K.J., Billington, S.L., (Eds.), Fracture Mechanics of Concrete and Concrete Structures – FraMCoS-5. Vail Colorado, pp. 255–262.

Kröner, E., 1968. Elasticity theory of materials with long-range cohesive force. International Journal of Solids and Structures 3, 731–742.

Jirásek, M., 1993. Modeling of fracture and damage in quasibrittle materials. PhD dissertation, Northwestern University, Evanston, IL.

Jirásek, M., Zimmermann, T., 1998. Rotating crack model with transition to scalar damage. Journal of Engineering Mechanics, ASCE 124 (3), 277–284.

Larsy, D., Belytschko, T., 1988. Localization limiter in transient problem. International Journal of Solids and Structure 24, 581–597.

Merlo, G., 2003. Il modello dei micropiani non-locale simmetrico applicato alla simulazione della propagazione della frattura nel calcestruzzo. Master Thesis, Department of Structural Engineering, Politecnico di Milano (in Italian).

Nooru-Mohamend, M.B., 1992. Mixed-mode fracture of concrete: an experimental approach. Doctoral Thesis Delft University of Thechnology, Delft, The Netherlands.

Ožbolt, J., Li, Y., Kozar, I., 2001. Microplane model for concrete with relaxed kinematic constraint. International Journal of Solids and Structures 38, 2683–2711.

Pijaudier-Cabot, G., Bažant, Z.P., 1987. Nonlocal damage theory. Journal of Engineering Mechanics, ASCE 113, 1512–1533.

Planas, J., Elices, M., Guinea, G.V., 1996. Basic issue of nonlocal models: uniaxial modeling. Technical Report 96-jp03, Universidad Politecnica de Madrid, Madrid, Spain.

Rambaldini, C., 1999. Valutazione della duttilita' di calcestruzzi fibrorinforzati. Master Thesis, University of Brescia (in Italian).

Saouridis, C., Mazars, J., 1992. Prediction of the failure and size effect in concrete via a bi-scale damage approach. Engineering Computations 9, 329–344.

Schlangen E., 1993. Experimental and numerical analysis of fracture processes in concrete. PhD Dissertation, TU Delft, Netherland.

Simone, A., 2003. Continuous–discontinuous modelling of failure. Doctoral Thesis Delft University of Technology, Delft, The Netherlands.

Strömberg, L., Ristinmaa, M., 1996. FE-formulation of a nonlocal plasticity theory. Computer Methods in Applied Mechanics and Engineering 136, 127–144.

Stroud, A.H., 1971. Approximate Calculation of Multiple Integrals. Prentice-Hall, Englewood Cliffs, NJ.

Taylor, G.I., 1938. Plastic strain in metals. Journal of the Institute of Metals 62, 307–324.

Vermeer, P.A., Brinkgreve, R.B.J., 1994. A new effective non-local strain measure for softening plasticity. In: Chambon, R., Desrues, J., Vardoulakis, I. (Eds.), Localization and Bifurcation Theory for Soil and Rocks. Balkema, Rotterdam, pp. 89–100.